# DEVELOPMENT OF A COMBINED MODEL OF TISSUE KINETICS AND RADIATION RESPONSE OF HUMAN BRONCHIOLAR EPITHELIUM WITH SINGLE CELL RESOLUTION

A Dissertation

by

NATELA GRIGORYEVNA OSTROVSKAYA

Submitted to the Office of Graduate Studies of
Texas A&M University
in partial fulfillment of the requirements for the degree of

DOCTOR OF PHILOSOPHY

August 2005

Major Subject: Nuclear Engineering

# DEVELOPMENT OF A COMBINED MODEL OF TISSUE KINETICS AND RADIATION RESPONSE OF HUMAN BRONCHIOLAR EPITHELIUM WITH SINGLE CELL RESOLUTION

A Dissertation

by

NATELA GRIGORYEVNA OSTROVSKAYA

Submitted to the Office of Graduate Studies of
Texas A&M University
in partial fulfillment of the requirements for the degree of

DOCTOR OF PHILOSOPHY

Approved by:

| | |
|---|---|
| Chair of Committee, | John R. Ford |
| Committee Members, | Leslie A. Braby |
| | Kenneth L. Peddicord |
| | Nancy Amato |
| Head of Department, | William E. Burchill |

August 2005

Major Subject: Nuclear Engineering

# ABSTRACT

Development of a Combined Model of Tissue Kinetics
and Radiation Response of Human Bronchiolar Epithelium
with Single Cell Resolution. (August 2005)
Natela Grigoryevna Ostrovskaya,
B.S., Obninsk Institute of Nuclear Power Engineering, Russia
Chair of Advisory Committee: Dr. John R. Ford

Lack of accurate data for epidemiological studies of low dose radiation effects necessitates development of dosimetric models allowing prediction of cancer risks for different organs. The objective of this work is to develop a model of the radiation response of human bronchiolar tissue with single cell resolution. The computer model describes epithelial tissue as an ensemble of individual cells, with the geometry of a human bronchiole and the properties of different cell types are taken into account. The model simulates the tissue kinetics and radiation exposure in four dimensions: three spatial dimensions and a temporal dimension.

The bronchiole is modeled as a regular hollow cylinder with the epithelial cells of three different types (basal, secretory, and ciliated) lining its interior. For the purposes of assessment of radiation damage to the cells only the nuclei of the cells have been modeled. Subroutines describing cellular kinetics have been developed to simulate cell turnover in a normal epithelial tissue. Monte Carlo subroutines have been developed to simulate exposure to alpha particles; the GEANT4 toolkit has been used to simulate

exposure to low LET radiation. Each hit cell is provided with a record of energy deposition, and this record is passed to the progeny if the cell survives.

The model output provides data on the number of basal progenitor cells in different phases of a cell life-cycle and secretory to ciliated cell ratio after several generations of cell proliferation. The model calculates labeling and mitotic indices and estimates the average cell turnover time for the bronchiolar tissue. Microdosimetric calculations are performed for cells traversed by ionizing particles. The model will be used to assess the accumulation of damage in cells due to protracted low level radiation exposure. The model output may provide directions for the future experimental design.

# ACKNOWLEDGMENTS

This research was supported by the Nuclear Engineering Research (NEER) Grant Program, U.S. Department of Energy, Grant No. DE-FG07-021D14329.

I would like to thank my committee chair, Dr. John Ford, for his guidance, tremendous support and encouragement throughout the course of this research, and for his dedication to his work and his students. I also want to extend my gratitude to Ms. Jan Rinehart for her friendship, support, and encouragement during my five years of study at Texas A&M University.

Special thanks to my family for their love, patience and encouragement.

# TABLE OF CONTENTS

# LIST OF FIGURES

FIGURE Page

# LIST OF TABLES

TABLE Page

# CHAPTER I

# INTRODUCTION

An exposure to ionizing radiation can cause deleterious effects in living organisms. The degree of the effect varies greatly depending on type of the exposure, dose, dose rate, and other factors. The most significant radiation-induced detrimental health effect is cancer. Numerous experiments with animals on induction of cancer by radioactive agents, studies of atomic bomb survivors in Japan, and analyses of data for occupational and medical exposures have provided evidence that radiation is a carcinogen. However, data used in these studies represented populations of animals or people exposed to acute doses of radiation. At background levels of exposure, induction of cancer is believed to be a rare event. However, it has been hypothesized that carcinogenesis is a multistep process and ionizing radiation is acknowledged to affect different stages of the process (*1-5*).

Ionizing radiation affects living matter by causing excitations and ionizations, which result in chemical changes in molecules. In a living cell, the nucleus, which stores the genetic information, is considered to be a critical target for radiation-induced damage. Passing through a cell nucleus, a radioactive particle can produce different types of damage in a DNA macromolecule. Powerful DNA damage-sensing machinery detects altered sites and triggers multi-protein complex DNA repair mechanisms to deal with radiation damage. Accurate repair is critical for normal cell functioning and

---

This dissertation follows the style of the *Radiation Research*.

proliferation. Both the complexity of DNA damage and the efficiency of DNA repair mechanisms determine cell fate. Failure to complete DNA repair and continue cell-cycle progression may lead to the induction of apoptosis (programmed cell death), which assures the removal of the compromised cell from the tissue. In case of fixation/misrepair of DNA damage, a cell may undergo permanent growth arrest resulting in loss of reproductive function and eventual death, or may remain in the proliferative compartment carrying a harmful genetic mutation and pass it on to progeny.

Over the past twenty years, experimental observations have revealed that ionizing radiation may also produce biological effects in cells that themselves were not irradiated. Chromosomal aberrations and gene mutations may arise in the progeny of the irradiated cells after many generations of cell division (*6-9*). Manifestation of these delayed effects in the descendants of irradiated cells is referred to as a phenomenon of "radiation-induced genomic instability". Another phenomenon that adds complexity to the low dose radiation risk assessment is "radiation-induced bystander effect", which refers to stress responses and genetic damage found in un-irradiated cells that are in contact with cells traversed by high-LET particles (*8-12*).

Estimation of low dose radiation risks remains a challenging problem (*13*). Lack of accurate data for epidemiological studies of low dose radiation effects necessitates development of dosimetric models allowing prediction of cancer risks for different organs. Since neoplastic transformation of a normal cell may require several independent mutations or epigenetic changes and the accumulation of a necessary number of alterations takes time, dosimetric models calculating only dose deposition to

a tissue may be not sufficient for risk assessment. Considering the fact that normal tissues can effectively stop a cell transition from normalcy to malignancy and an abnormal tissue can promote development of cancerous cells (*14*), it is important to model tissue as an ensemble of individual but interdependent cells. Radiation-induced delays in a cell-cycle progression and variation in cell sensitivity to the radiation exposure in different cell-cycle phases make the cellular kinetics an important part of a dosimetric model (*15-17*). Finally, possible proliferation of an affected cell and the passing of genetic mutations to the progeny necessitate the tracing of the accumulation of potentially harmful events in a single cell lineage. This is the problem that will be the focus of this dissertation.

# CHAPTER II

# PROBLEM

## *Present Status of the Question*

A number of dosimetric models have been developed to estimate the absorbed dose in different organs, including tissues of the respiratory tract that are of the most interest for this work. Most of the models deal with calculation of the absorbed dose to different cells of the airways due to internal exposure to α-particle emitters, e.g. radon. Inhalation of radon, a colorless and odorless gas, one of the products of the decay of uranium which occurs naturally in the earth's crust, is the second major cause of lung cancer after smoking (*18*).

Mercer and co-workers developed a cylindrical tissue model for calculation of absorbed dose from Po-218 and Po-214 inhaled alpha particles for cells populating human and rat airways (*19*). They assumed that the source of α particles with activity of 1 dpm was uniformly distributed in the mucous layer and used the measurements of epithelial thickness and volume density to estimate the energy absorbed by nuclei of different cell types located at different depths from the epithelial surface.

Harley *et al.* derived a biological model to assess risk of lung cancer induction following exposure to Rn-222 (*20*). They assumed that cycling cells in the bronchial epithelium were the primary targets for carcinogenesis. The model incorporated expressions for the deposition of Rn-222 decay products in the bronchial airways, number of alpha particle traversals and energy deposition to the bronchial epithelial cells, and morphometric data for generations 2-6 of the bronchial tree obtained and reported by others. The model allowed estimating the total number of cycling cells

traversed by an alpha particle for an exposure of 1 WLM and calculating the number of dividing cells as a function of time after exposure.

Nikezic *et al.* used cylindrical geometry in the development of a semi-analytical method for calculation the absorbed dose delivered by alpha particles to the sensitive cells of the airways (*21*). The airway tube was represented by a cylinder with given radius of the lumen. The source of α-particles was distributed in the cylindrical section representing the mucous. The energy deposited to a small sphere located at some depth in the tissue was calculated. Nikezic and co-workers considered the near-wall case, when the particle emitted traveled only in the tissue, and the far-wall case, when alpha particle passed through the air cavity before it reached the sphere of interest. This method allowed calculating dose conversion coefficients and absorbed fractions of alpha particles in the sensitive cells of the bronchial and bronchiolar regions of the respiratory tract. The results obtained were in good agreement with values produced by NRC and ICRP66 models.

Recently, Nikezic and Yu have calculated the distribution of specific energy in the sensitive layers of the human respiratory tract using the concept of an effective volume in a tissue (*22*). The effective volume for a point of interest (target) was represented by a sphere; the radius of the sphere was chosen to be equal to the particle range in the medium. Only alpha particles originated in the effective volume had non-zero probability of hitting the target, which was placed in the center of the effective volume. The authors used Monte Carlo method to calculate the probability density distribution of specific energy for one event for bronchial and bronchiolar epithelium. Later, Nikezic and Yu have also developed a model for bifurcation regions of the

human tracheobronchial tree, which was used to calculate the absorbed fractions of alpha particles emitted in the region (*23*). Only alpha particles originated in the bifurcation region were considered. As in previous study, the radio-nuclides were uniformly distributed in the mucus. The authors found that the absorbed fractions were up to 20% larger in the bronchiolar bifurcation regions compared to the straight cylindrical regions.

Stewart and Traub used three-dimensional tissue constructs to calculate tumor control probabilities (*24*). To model a tumor with heterogeneous biophysical properties, such as non-uniform distribution of radioresistant and radiosensitive cells, a cylindrical tissue construct was subdivided into thousands of annular voxels. The MCNP Monte Carlo code was employed to simulate 1 MeV photon broad-beam irradiation of a cylindrical tissue construct. The absorbed dose distributions were calculated and cell survival fractions were estimated for each tissue region using the Lethal and Potentially Lethal radiobiological model.

Chauvie *et al.* developed a Monte Carlo model to estimate cell survival in hadrontherapy (*25*). The simulated asynchronous populations of CHO and V79 cells (as monolayer) irradiated with 11 and 270 MeV/nucleon carbon ions, respectively. The authors used the Geant Monte Carlo toolkit to simulate the energy deposition to the cells.

*Problem Formulation*

All of the dosimetric models described above are essentially static, which assumes no tissue kinetic processes, e.g. cell proliferation. The novelty of the proposed

approach is to build the tissue construct from bottom up, cell by cell, taking into account geometric and morphometric parameters of human bronchioles and cells populating the bronchiolar epithelium. The model should describe the bronchiolar epithelial tissue kinetics and allow simulating the long term exposure to ionizing radiation.

Human bronchiolar epithelium was selected as a tissue of interest due to following reasons:

- the lung epithelial tissue plays an important role in normal lung physiology.
- lung epithelia are target tissues for occupational internal exposures and for radon exposure (*26*);
- the epithelium of bronchioles appears to be the origin of the pulmonary tumors induced by radioactive agents (*27-29*); in populations exposed only to background level of radiation one-fifth of the squamous cell and small cell carcinomas, three-fourths of the adenocarcinomas, and one-half of all large cell cancers are assumed to originate in the bronchioles (*18*);
- histological and morphological data for human bronchiolar epithelial tissue and data on cell proliferation rates are available in the literature and may be used for incorporation into the model (*30-32*).

Human bronchioles are 9th to 14th generation branches of the bronchial tree extending into the lung (*18*). The main function of this part of the respiratory system is to conduct the air into and out of the respiratory region. The shape of a bronchiole can be represented by a hollow cylinder, with the epithelial layer lining the interior of the cylinder (Fig. 1).

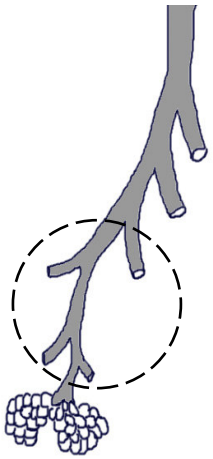

**FIG. 1**. Bronchioles.

Three major cell types populating the bronchiolar epithelium are basal, secretory, and ciliated ones. Secretory cells are tall dome-shaped cells that synthesize, store and secrete protein components of extracellular lining of the bronchiole. Ciliated cells have cuboidal or tall columnar shape. Each ciliated cell has about three hundred cilia that beat in a coordinated fashion toward trachea in order to move mucus and trapped particulates toward pharynx. Nuclei of secretory and ciliated cell can be described as ellipsoids. Basal cells have a bell-shaped structure. The nucleus of the basal cell occupies the essential part of the cellular volume and can be presented by a sphere. Basal cells are shorter than ciliated and secretory cells; they rest on the basal lamina and do not reach the lumen of the bronchiole. Due to this difference in cellular height, the bronchiolar epithelium has a pseudo-stratified structure.

# CHAPTER III

# METHODS

A software model of human bronchiolar epithelial tissue kinetics and radiation response has been implemented in C++ programming language using Microsoft Visual C++ .NET development environment. The model development consists of four steps:

1. Modeling of the geometry of the bronchiole and its epithelial tissue.
2. Modeling of the tissue kinetics.
3. Modeling of the radiation exposure.
4. Modeling of the radiation response.

## *Bronchiole Construction*

A three-dimensional model of human bronchiole has been implemented. The bronchiole is modeled as a regular hollow cylinder with the epithelial cells lining its interior (*31, 32*). The cell types constituting the bronchiolar epithelium are basal (stem and non-stem), secretory, and ciliated. The average caliber of the bronchiolar wall, the pseudo-stratified structure of the bronchiolar epithelium, the average thicknesses of mucous and cilia layers, the average thickness of epithelium, the average depth of nuclei of cells at risk, and the morphometric parameters of the epithelial cells are taken into account (*18, 33-35*). The approach implemented in this model assumes that for the purposes of assessment of radiation damage to the cells only the nuclei of the cells considered.

Construction of the bronchiole starts with building the basal cell layer. The nuclei of the basal cells are randomly assigned positions on the wall of the regular

cylinder taking into account the mean cell diameters and the positions of the nuclei in the cells. To do this, a regular hexagonal grid is developed and superimposed on the cylinder wall. The size of the hexagonal cell is larger than the size of the basal cell, therefore each hexagon of the grid represents region that can contain one and only one basal cell. The nucleus of a basal cell is placed in the center of each hexagonal region, ensuring that basal cells are distributed on the wall of the bronchiole. Then, the position of each nucleus is altered within the hexagonal region (Fig. 2A). As a result, an irregular (random) grid for the nuclei of the basal cells is built. Next, a special subroutine defines which nodes of the "basal grid" contain pluripotent stem cells. The subroutine assures that no two stem cells are neighbors (Fig. 2B).

A second hexagonal grid is superimposed above the basal cell layer to locate superficial secretory and ciliated cells (Fig. 3A). It is assumed that shape of columnar

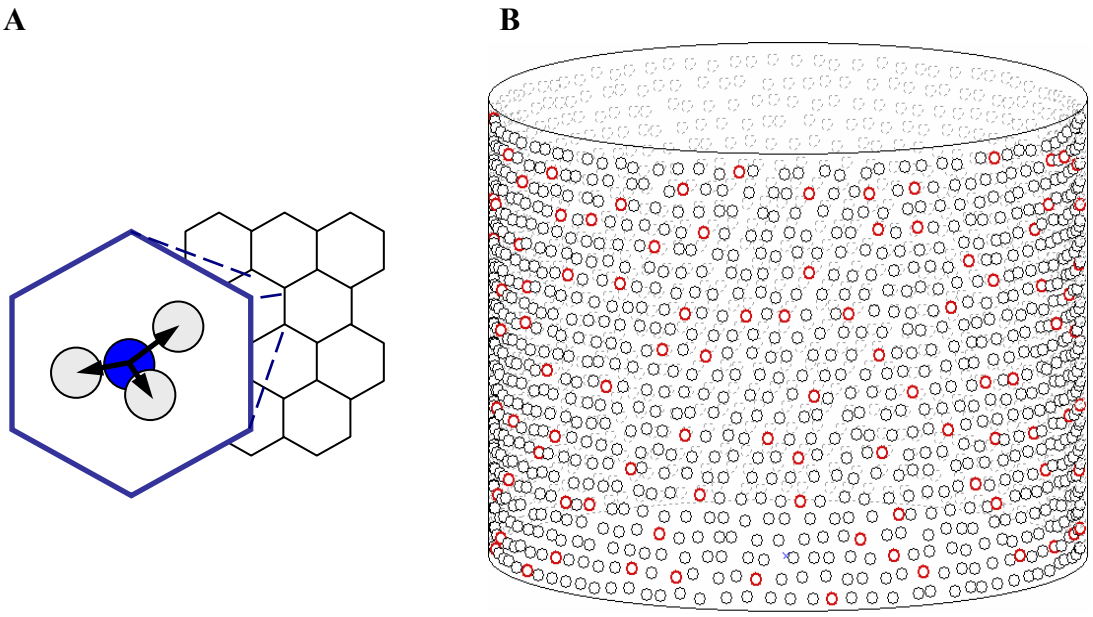


**FIG. 2.** Construction of the basal cell layer. Panel A: Positioning of a basal cell nucleus in a hexagonal region. Panel B: Irregular basal cell grid, stem cells are marked with red circles.

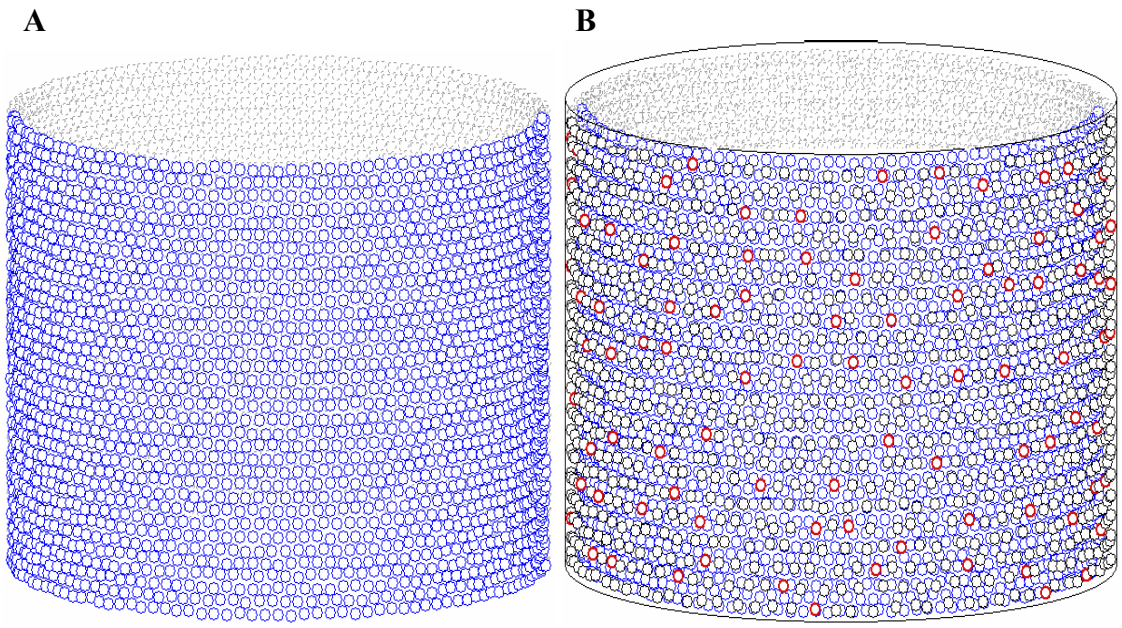


**FIG. 3.** Construction of the bronchiole. Panel A: Secretory and ciliated cells grid. Panel B: Completed bronchiole construct.

secretory or ciliated cells can be considered hexagonal in cross-section, and the cell occupies the whole hexagon in the grid. The nuclei are essentially centered relative to the vertical walls of the cells. The nucleus of the cell is centered in the hexagonal volume and then its position is slightly altered, using the algorithm developed for the basal cells. The fact that the nuclei do not all lie at the same depth is taken into account. Morphometric parameters for the airway and basal, secretory and ciliated cells are summarized in Table 1. When all the geometric locations for potential cells are defined, the bronchiole construct is generated (Fig. 3B) and ready to be populated with "living" cells to create a "live" epithelial tissue.

**TABLE 1**
**Morphometric parameters for bronchiole and basal, secretory and ciliated cells**

| Parameter | Value, μm |
|---|---|
| Airway diameter, generation 14 (13) | 603 (720)[a] |
| Airway height, generation 14 (13) | 1700 (2069)[a] |
| Thickness of epithelium | 30[a] |
| Thickness of mucous layer | 5[a] |
| Basal cell region diameter[b] | 22 |
| Basal cell nucleus diameter, nucleus shape – sphere | 5 – 8[c] |
| Secretory/ciliated cell diameter[b] | 14 |
| Secretory/ciliated cell nucleus semiaxes, nucleus shape – ellipsoid | 6, 4, 4 |

[a] From Table 2 in *Publication 66* (ICRP, 1994) (*18*).
[b] The diameter of the circle inscribed in the hexagon of the grid.
[c] Mercer *et al.* (*33*).

*Tissue Kinetics*

Subroutines describing cellular kinetics - birth, growth, differentiation, proliferation, and death have been developed to simulate cell turnover in the bronchiolar epithelium. The model assumes that in a normally functioning bronchiolar epithelial tissue there are two compartments representing different cell subpopulations: proliferating and functional. These compartments are distinguished by cell type and cell functions.

*Proliferative compartment*. The proliferative compartment comprises basal cells that have the potential to divide and to produce daughter cells of all types: basal, secretory, and ciliated (*36-39*). This compartment contains active (cycling) cells and non-active (resting) cells. Resting cells may undergo mitosis if stimulated somehow,

e.g. from the extracellular environment or by signals from the adjacent cells, to enter the cell cycle. Basal cells include both stem and non-stem cells. Stem cells are pluripotent cells distinguished by unlimited proliferative potential. They can give rise to any cell in the bronchiolar tissue: stem or non-stem basal cell, secretory or ciliated cell (*40*). Non-stem basal cell can give rise to another non-stem basal cell, or produce an intermediate daughter cell that differentiates into secretory or ciliated cell. It is assumed that the differentiation of the intermediate cell occurs immediately. The schematic diagram of cell proliferation is presented in Figure 4. Basal cells comprise approximately 30 % of the total cell population in the bronchiolar epithelium (*34, 41)*. Research data on cell replacement and proliferation suggest that stem cells constitute up to 3% of the total epithelial cells, or about 10 % of the total basal cell population (*40, 42, 43*). The model assumes that stem cells are evenly distributed in the bronchiolar epithelium. Proliferating basal cells go through a cell cycle, which consists of five phases: $G_0/G_1$ (rest/growth), S (DNA synthesis), $G_2$ (growth), and M (mitosis). The progression of a basal cell through the cell cycle is depicted in Figure 5.

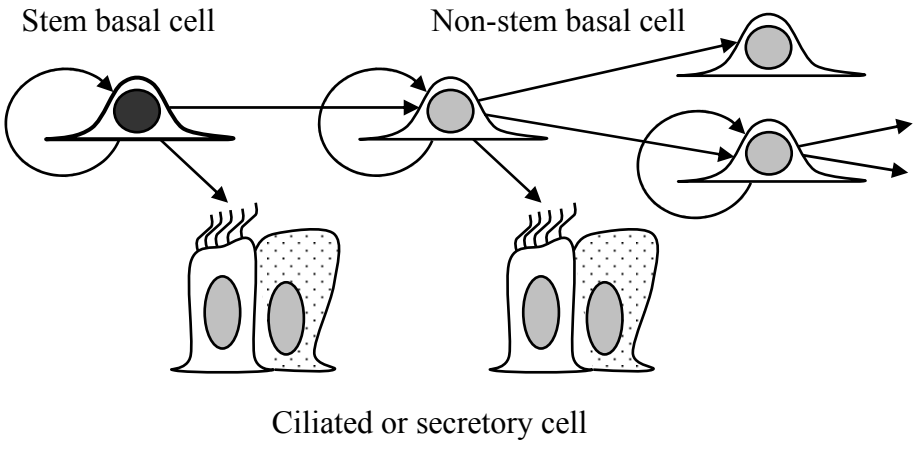


**FIG. 4.** Proposed scheme of cell proliferation.

A data structure describing basal cells has been created. The structure `BasalCell` contains fields that provide information on cell's lifetime clock position, cell-cycle clock position and duration of each cell-cycle phase (except for the $G_0$-phase), 'stemness' (whether the cell is a stem or a non-stem one), proliferative capacity, type of death, and cell generation in the lineage. The lifetime of a non-stem basal cell is defined by the proliferative capacity of the cell: the basal cell does not die until it depletes the number of possible divisions. The number of possible divisions for the cell is a random quantity described by a Poisson distribution with a mean of three cell doublings, and is determined when the cell is born. The model assumes that a non-stem basal cell can divide up to 8 times. Stem cells are assigned an "unlimited" number (e.g. one million) of divisions. They are considered to cycle slower than non-stem cells (longer $G_1$-phase) and they divide only when non-stem cells cannot replenish dying cells in a timely manner. Stem cells are modeled as mortal cells, however their lifespan is much longer compared to the non-stem cells.

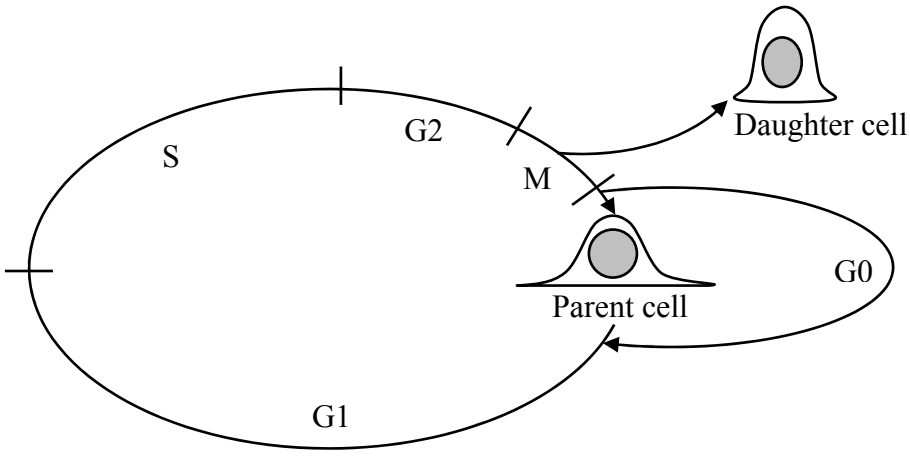


**FIG. 5.** Basal cell-cycle progression.

*Duration of cell cycle phases*. The model allows adjusting the duration of each cell cycle phase (except for $G_0$-phase). The duration of the S-phase of the cell cycle, DNA synthesis, is estimated from the experimental data reported by other researchers (*44, 45*). The length of the $G_2$-phase is about 4 hours, while M-phase is the shortest phase in the cycle and lasts about one hour (*46*). The following values were chosen for the duration of the cycle phases of a non-stem basal cell: $G_1$-non-stem – 24 h, $G_1$-stem – 48 h, S – 8-10 h, $G_2$ – 2-4 h, and M – 2 h. The model assumes that the duration of S-phase, G2-phase, and M-phase cannot change under normal conditions. The duration of the $G_1$-phase can vary due to the fact that cell growth is governed by circadian rhythms (discussed below).

*Mitotic inhibition*. Research data suggest that inhibition of cell growth and division in normal tissues is possible and can be triggered by high cell density (*47-50*). The mechanism of mitotic inhibition is implemented in the model for proliferative cells. A basal cell possessing a non-zero proliferative potential stays in $G_0$-phase (rest) and cannot enter cell cycle if all adjacent hexagons in the basal and secretory/ciliated grids are occupied by living cells. The basal cell can start to cycle when at least one of the neighboring cells dies or is determined to die within a time period, which is shorter than the duration of the cell cycle of the basal cell in question.

*Circadian rhythms*. It is well established that progression of proliferating cells through the cell cycle is influenced by circadian rhythms (*51-55*). Human cells synthesize DNA (S-phase) more actively during the daytime and show higher mitotic activity (M-phase) in the night (*56*). Circadian oscillations of the fraction of basal cells in mitosis can be approximately described by a periodic function, e.g. sinusoid or co-

sinusoid. In the model, circadian variation of the mitotic activity (*MA*) is described by the following function:

$$f_{MA}(x) = a\cos(x) + b \tag{1}$$

where $x \in [0, 2\pi)$,

$a$ – amplitude control coefficient,

$b$ – constant, which is used to ensure that the $f_{MA}(x)$ does not take negative values, $b \geq a$.

The amplitude of the circadian rhythm variation can be adjusted by varying the amplitude control coefficient $a$ in the Equation (1).

Let T denote the time of the day when a basal cell undergoes mitosis, T is a discrete random variable defined on the set of integers $\{0, \ldots, 23\}$. To implement the circadian variation of the mitotic activity into the model, a probability mass function is constructed in the following manner. The area under the curve described by the Equation (1) is calculated for $x \in [0, 2\pi]$ and normalized to unity. Next, the area is divided into twenty four segments corresponding to the number of hours in a day; width of each segment is taken to be $2\pi/24$. Thus, the probability that a basal cell undergoes mitosis at time $t$ is calculated as

$$P\{T = t\} = \frac{\int_{\pi t/12}^{\pi(t+1)/12} f_{MA}(x)dx}{\int_{0}^{2\pi} f_{MA}(x)dx} \tag{2}$$

As a result, the discrete random variable T with the distribution

$$T = \begin{pmatrix} t_0 & t_1 & \dots & t_{23} \\ p_0 & p_1 & \dots & p_{23} \end{pmatrix} = \begin{pmatrix} 0 & 1 & \dots & 23 \\ p_0 & p_1 & \dots & p_{23} \end{pmatrix}$$

where $p_i$ - the area of the $i$-th area segment,

$i = 0..23$,

$\sum p_i = 1$,

is constructed. The program generates a random variable $\xi$ uniformly distributed over [0, 1]. The basal cell will undergo mitosis at time of the day $T = t_i$ whenever

$$p_1 + p_2 + \dots + p_{i-1} \leq \xi < p_1 + p_2 + \dots + p_i.$$

Before a basal cell starts the $G_1$-phase of the cell cycle, the program calculates the time of the potential mitosis defined by the circadian rhythm and adjusts the duration of the $G_1$-phase accordingly.

*Functional compartment.* The functional compartment includes columnar secretory and ciliated cells that carry out particular functions in the epithelial tissue. Although, some experimental reports suggest that secretory cells can proliferate, the model does not assign this ability to the secretory cells. Secretory and ciliated cells are considered to be terminally differentiated and therefore cannot undergo cell cycle progression (*39, 40*). Secretory and ciliated cells, in approximately equal proportions, comprise approximately 70 % of the total cell population in the bronchiolar epithelium (*34, 41*).

A data structure describing both secretory and ciliated cells has been created. The structure `CilSecCell` contains fields that provide information on cell's type

(secretory or ciliated), cell's lifetime clock position, type of death, cell generation in the lineage, and record of the parent basal cell identifier. The model allows the adjustment of the duration of the life span of the secretory/ciliated cells. The model assumes that the lifetime of a secretory/ciliated cell varies from 7 to 12 days.

*Cell death.* The model assumes that aged epithelial cells, i.e. cells with a zero lifespan, die by programmed cell death (apoptosis). Apoptosis is a fast and clean mechanism of removal of unwanted cells from the tissue and plays an important role in maintaining tissue homeostasis (*57, 58*). Apoptosis can occur, for instance, when a cell is infected with a virus. In addition to cellular death due to aging, the model allows simulating a faulty event in a young cell (e.g. viral infection) that leads to a lethal outcome. In this case, the cell dies by apoptosis. For non-irradiated epithelial tissue, two types of cell death are distinguished by the model: apoptosis due to aging and apoptosis triggered by an unfortunate event in the cell.

*Modeling of the Radiation Exposure*

Internal radiation exposure has been simulated for both high-LET (α-particles) and low-LET (photons) radiations. The model assumes that initially all radioactive particles are deposited and uniformly distributed in the mucociliary layer of the bronchiole. The geometry of the mucociliary layer is defined as the region bounded by two concentric cylinders: the radius of the first cylinder, $R_1$, is equal to the radius of the bronchiole lumen; the radius of the second cylinder, $R_2$, is equal to $R_1$ plus thickness of the mucociliary layer.

For the purposes of simulation of radioactive particles' transport in the bronchiole and for the determination of specific energies deposited in the epithelial cells, the elemental composition and density of muscle striated tissue was adopted from ICRU Report 44 and Berger *et al*. (*59, 60*). The lumen of the bronchiole is assumed to be filled with dry air described by the elemental composition suggested by Berger *et al*. (*60*).

To trace the accumulation of potentially harmful events in a cell, each hit cell is provided with a record of energy deposition, and this record is propagated to the progeny of a hit cell if the cell survives. Both structures **`BasalCell`** and **`CilSecCell`** contain data fields that store information on energy deposition in the hit cell nucleus, number of hits for the cell, energy deposition in the nucleus of the immediate parent cell, number of hits for the immediate parent cell, number of hit cells in the cell lineage, and number of cells in the lineage that received multiple hits.

*Exposure to α-particles*. The Monte Carlo method has been used to simulate the exposure to α-particles. The point of origin of an α-particle, $P_\alpha(\rho, \varphi, z)$, is sampled randomly in the following manner:

$$\begin{aligned} \rho &= R_1 + \xi_1 T_{ML} \\ \varphi &= 2\pi\xi_2 \\ z &= \xi_3 H_B \end{aligned} \qquad (3)$$

where $\rho, \varphi, z$ - coordinates of $P_\alpha$ in the cylindrical coordinate system,

$\xi_1, \xi_2, \xi_3$ - random variables uniformly distributed over [0, 1],

$T_{ML}$ - thickness of the mucociliary layer,

$H_B$ - height of the bronchiole.

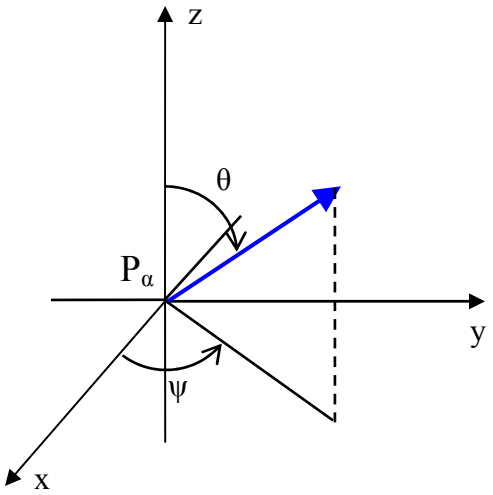


**FIG. 6.** Choice of random direction of α-particle emission.
ψ varies from 0 to 2π, θ varies from 0 to π.

The track of an α-particle is modeled as a straight line. The direction of the flight is selected randomly (Fig. 6); directional cosines α, β, γ, are calculated as follows:

$$\alpha = \cos(\psi)\sin(\theta)$$

$$\beta = \sin(\psi)\sin(\theta) \qquad (4)$$

$$\gamma = \cos(\theta)$$

where $\psi = 2\pi\zeta_1$,

$\theta = \pi\zeta_2$,

$\zeta_1$, $\zeta_2$ - random variables uniformly distributed over [0, 1].

*Range of α-particles in the bronchiole.* The model assumes that α-particles lose their kinetic energy gradually accordingly to the continuous slowing-down approximation (CSDA). Data for α-particle CSDA ranges, as a function of energy, in the epithelial tissue and in the air were adopted from Berger *et al*. and ICRU Report 49 (*60, 61*). The range versus energy and the energy versus range curves were plotted and

the fitting functions were obtained using MS Excel. When an α-particle is emitted, three scenarios are possible:

1. The α-particle enters the lumen of the bronchiole and comes to rest in the lumen (Fig.7A).
2. The α-particle passes through the lumen and reenters the epithelium (Fig.7B).
3. The α-particle does not enter the lumen; it travels entirely within the bronchiolar epithelial tissue: the particle may stop in the bronchiole or may reach the outer wall of the bronchiole and leave (Fig.7C).

When the α-particle enters the lumen of the bronchiole, the range of the particle is recalculated to account for the composition of the lumen. If the α-particle reenters the bronchiolar epithelium, the range is recalculated again for the epithelial tissue.

*Dosimetry of α–particles in the epithelial cells.* During the course of α-particle track simulation, the program finds all epithelial cells hit by the particle. The energy

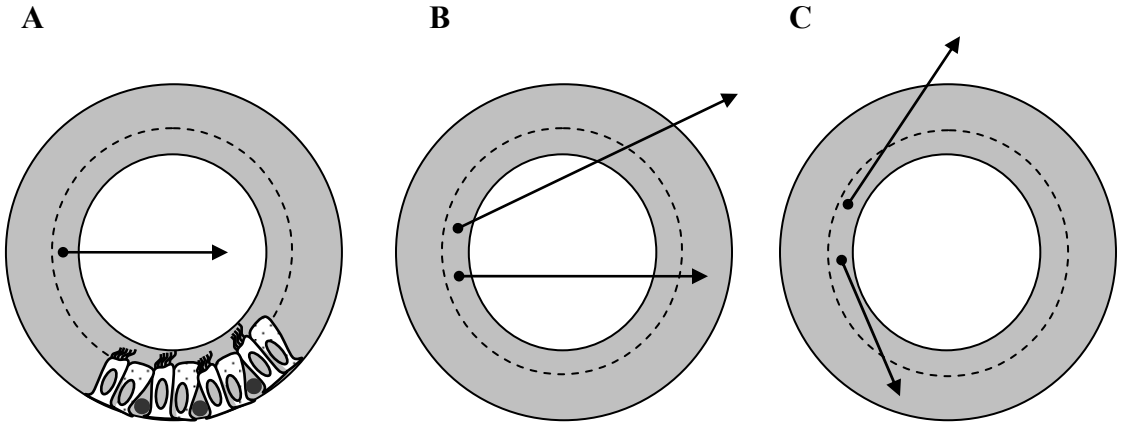


**FIG. 7.** Path of an α-particle in the bronchiole. Panel A: α particle enters the bronchiole lumen of and comes to rest. Panel B: α particle passes through the lumen and reenters the epithelium of the bronchiole. Panel C: α particle does not enter the lumen; the particle stops in the epithelium or leaves the bronchiole.

deposited in a hit cell nucleus is calculated as the difference between the 'entering into the nucleus' and the 'exiting from the nucleus' (or 'stopping in the nucleus') energies of the particle. Also, the length of the α-particle path through the cell nucleus is calculated.

*Exposure to low-LET radiations*. A separate software module has been developed to model exposure of the bronchiolar epithelium to low-LET radiations (photons and electrons). Since the independent development of a code for the Monte Carlo simulation of coupled photon-electron transport or electron transport alone is a time and personnel intensive task, we elected to use one of the industrial packages available for simulation of particle transport in materials.

The module was developed using the Geant4 toolkit, a powerful software package designed for the Monte Carlo simulation of particle transport and interactions with matter (*62*). The toolkit provides means to create a model of the object in question with a desired geometrical shape, dimensions, and material composition. A comprehensive set of physics processes is available for modeling the interaction of particles with the composite material. The Geant4 code allows the user to define a sensitive region (a detector volume) in the modeled object. When a particle travels in the detector volume, the information on the type of interactions, geometrical position and time of the events, and the energy deposition along the particle track is available.

The Geant4 code uses condensed simulation algorithms for particle tracking, where the effects of the interactions (energy deposition events) are summarized at the end of a track segment. The length of the particle range for a single path step was set to one micron, which is the smallest resolvable distance in the basal and the

secretory/ciliated hexagonal grids in the main simulation. Thus, the accuracy of the condensed history algorithm for particle tracking in matter is performed at the maximum resolution of the simulation.

Since photons and energetic electrons can travel distances that are much larger than the dimensions of the bronchiole, it is necessary to check if particles generated elsewhere in the lungs can reach and hit the epithelial cells of the bronchiole in question. To implement this, the approximate model of the human lungs and the rib cage was constructed (Fig. 8A). The geometry and dimensions of the lungs and the rib cage were partially adopted from the adult phantom developed in Oak Ridge National Lab (*63*).

Each lung is represented by half of an ellipsoid and defined as follows:

$$\begin{cases} \left(\frac{x \pm x_0}{a}\right)^2 + \left(\frac{y}{b}\right)^2 + \left(\frac{z - z_0}{c}\right)^2 \le 1 \\ z \ge z_0 \end{cases} \tag{5}$$

where $a$ = 7.5 cm, $b$ = 5 cm, $c$ = 24 cm, $x_0$ = 8.5 cm, $z_0$ = 13.4 cm. The elemental composition and density of the lung tissue was adopted from ICRU Report 46 to specify the composite material of the lung ellipsoids (*64*).

To construct the rib cage, each rib was defined as a volume between two concentric elliptical cylinders and two horizontal planes as follows:

$$\begin{cases} \left(\frac{x}{a_1}\right)^2 + \left(\frac{y}{b_1}\right)^2 \le 1 \\ \left(\frac{x}{a_2}\right)^2 + \left(\frac{y}{b_2}\right)^2 \le 1 \\ z_1 \le z \le z_2 \end{cases} \tag{6}$$

**TABLE 2**
**Rib cage parameters**

| Rib # | $a_1$ (cm) | $b_1$ (cm) | $a_2$ (cm) | $b_2$ (cm) | $z_1$ (cm) | $z_2$ (cm) |
|---|---|---|---|---|---|---|
| 1 | 13.5 | 6.3 | 14.0 | 6.8 | 36.5 | 37.9 |
| 2 | 14.0 | 6.8 | 14.5 | 7.3 | 33.7 | 35.1 |
| 3 | 14.5 | 7.3 | 15.0 | 7.8 | 30.9 | 32.3 |
| 4 | 15.0 | 7.8 | 15.5 | 8.3 | 28.1 | 29.5 |
| 5 | 15.5 | 8.3 | 16.0 | 8.8 | 25.3 | 26.7 |
| 6 | 16.0 | 8.8 | 16.5 | 9.3 | 22.5 | 23.9 |
| 7 | 16.5 | 9.3 | 17.0 | 9.8 | 19.7 | 21.1 |
| 8 | 16.5 | 9.3 | 17.0 | 9.8 | 16.9 | 18.3 |
| 9 | 16.5 | 9.3 | 17.0 | 9.8 | 14.1 | 15.5 |
| 10 | 16.5 | 9.3 | 17.0 | 9.8 | 11.3 | 12.7 |
| 11 | 16.5 | 9.3 | 17.0 | 9.8 | 8.5 | 9.9 |
| 12 | 16.5 | 9.3 | 17.0 | 9.8 | 5.7 | 7.1 |

where values for parameters $a_1$, $b_1$, $a_2$, $b_2$, $z_1$, and $z_2$ are listed in Table 2. The elemental compositions and densities of the skeleton-ribs ($2^{nd}$, $6^{th}$) and skeleton-ribs ($10^{th}$) tissues were adopted from ICRU Report 46 to specify the composite material of the rib volumes (*64*). The ribs 1 – 9 were assigned the elemental composition of the skeleton-ribs ($2^{nd}$, $6^{th}$) tissue; the ribs 10 – 12 were assigned the elemental composition of the skeleton-ribs ($10^{th}$) tissue. The volume between the ribs and the lungs is assumed to have the same elemental composition as the striated muscle tissue.

The construction of the bronchiole in the Geant4 module is different from how it was done in the main program. The bronchiole is defined by two concentric cylinders representing the epithelial tissue. The cell nuclei are not modeled. The lumen of the bronchiole is modeled as a separate cylinder to allow specifying the air as a material. The diameter and the height of the bronchiole, the thicknesses of the epithelium and the

mucociliary layer, the elemental compositions and densities of the bronchiolar tissue and the air in the lumen are exactly the same as in the main program. The epithelial layer of the bronchiole excluding the mucociliary layer is specified as the detector volume. The bronchiole is randomly placed in the lungs (Fig. 8B).

The model assumes that the total activity in the lungs is proportional to the activity of the particles deposited in the bronchiole. The total activity in the lungs is calculated using the surface activity in the bronchiole and the surface areas of bronchi and non-respiratory bronchioles (*18*). The number of particles needed for the simulation of the long-term internal exposure is generated. Each particle is tracked till it comes to rest and the information on the events of energy deposition in the epithelial layer of the bronchiole is stored in a file in a string format. Each string contains the identifier of the

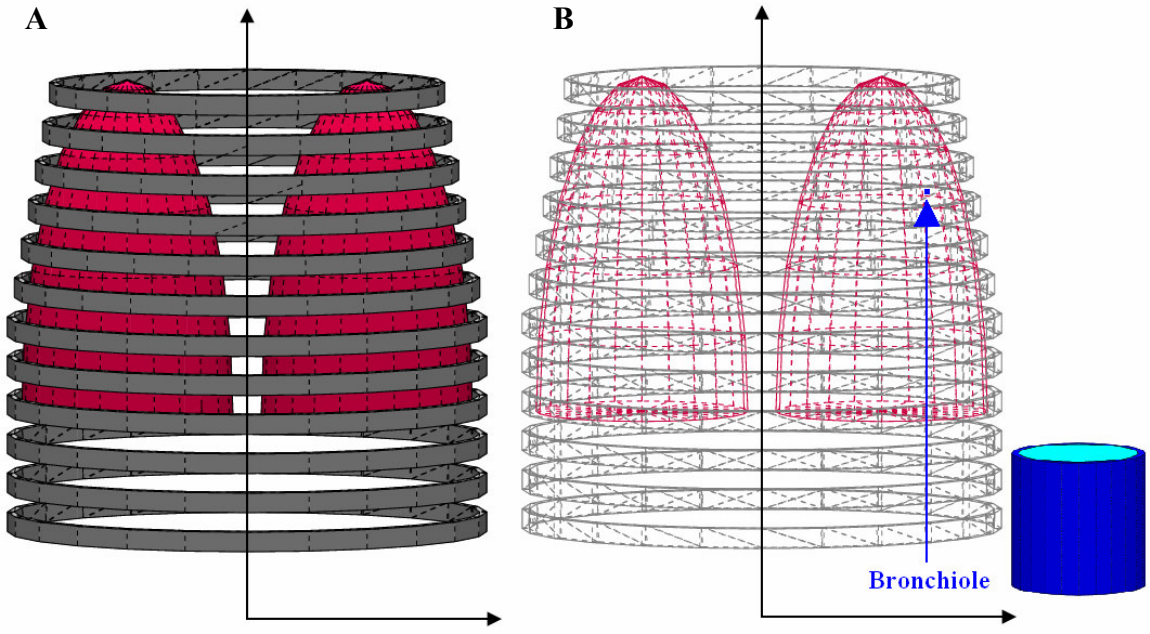


**FIG. 8.** The approximate model of human lungs and rib cage. Panel A: Lungs and rib cage constructs. Panel B: Placement of the bronchiole in the lungs.

primary particle, the coordinates of the energy deposition point, and the amount of energy deposited in that point. Later, the main program parses this file to retrieve data for the energy deposition events and to identify the epithelial cells traversed by radioactive particles.

*Modeling of the Radiation Response*

Cells traversed by ionizing particles may respond differently to a particular radiation insult. Cellular response depends on both the magnitude of the damage produced by radiation and the cell type. Proliferating cells may pause in their cell-cycle progression to allow sufficient time for repair of DNA lesions. Cell-cycle arrest has been observed in $G_1$, S, and $G_2$ phases for a range of different cells (*65-68*). Radiation exposure may also lead to permanent growth arrest resulting in loss of reproductive capacity by the injured cell (*69*). When damage produced by radiation is beyond repair, apoptosis may be triggered to remove the severely damaged cell from the tissue (*70, 71*). If a proliferating cell is damaged while transiting the M-phase (mitosis) of the cell cycle, the cell is not capable of repair and undergoes mitotic death (*72*). The model allows the simulation of all of these processes: cell-cycle arrest, cellular repair, loss of reproductive capacity, mitotic death, and finally radiation-induced apoptosis.

For each traversed cell, the amount of energy deposited in the nucleus by ionization is calculated. If energy deposition is greater than a lethal threshold, the hit cell dies by apoptosis within one simulated hour. The lethal threshold is defined as the amount of energy needed for the immediate inactivation of a cell. The lethal threshold is calculated as the energy deposited in the cell nucleus by a 100 keV/μm LET particle with the path length equal to one quarter of the cell nucleus diameter, which is close to

the value suggested by Griffiths *et al.* (*73*). The model assumes that basal, ciliated, and secretory cells respond similarly to a lethal amount of deposited energy. When energy deposited in the cell's nucleus is less than the lethal threshold, basal cells follow a more complex behavioral scenario than ciliated and secretory cells (see Figure 9 and 10). This is explained by the fact that basal cells can proliferate and, hence, are distributed through the phases of the cell cycle.

*Radiation response of ciliated and secretory cells*. In the event that the energy deposited in the cell nucleus is not lethal, ciliated and secretory cells will attempt to repair the damage produced by radiation. If the repair is effective, the cell continues living and functioning normally in the tissue. Otherwise, apoptosis is induced and the cell dies within one simulated hour (Fig. 9). To estimate the approximate probability of the efficient repair, the data for cell survival following exposure to α-particles and X-rays were adopted from Hall (*74*) and analytical expressions were obtained:

$$P_{\gamma}(D) = \exp(-0.12D - 0.04D^2) \tag{6}$$

$$P_{\alpha}(D) = \exp(-1.74D) \tag{7}$$

where $P_{\gamma}$ and $P_{\alpha}$ are repair probabilities for exposures to γ- and α-radiations respectively, and $D$ equals the dose to the cell nucleus.

*Radiation response of basal cells.* Basal cells follow more complex paths responding to radiation damage (Fig. 10). They may undergo cell cycle arrest, repair, reproductive failure, mitotic death, and apoptosis. For cycling basal cells, two forms of apoptosis are recognized: premitotic and postmitotic (*71*).

*Cell cycle arrest.* Following a radiation insult in either the $G_1$-, S-, or $G_2$-phase of the cycle, a basal cell may induce cell cycle arrest to allow time for repair of DNA

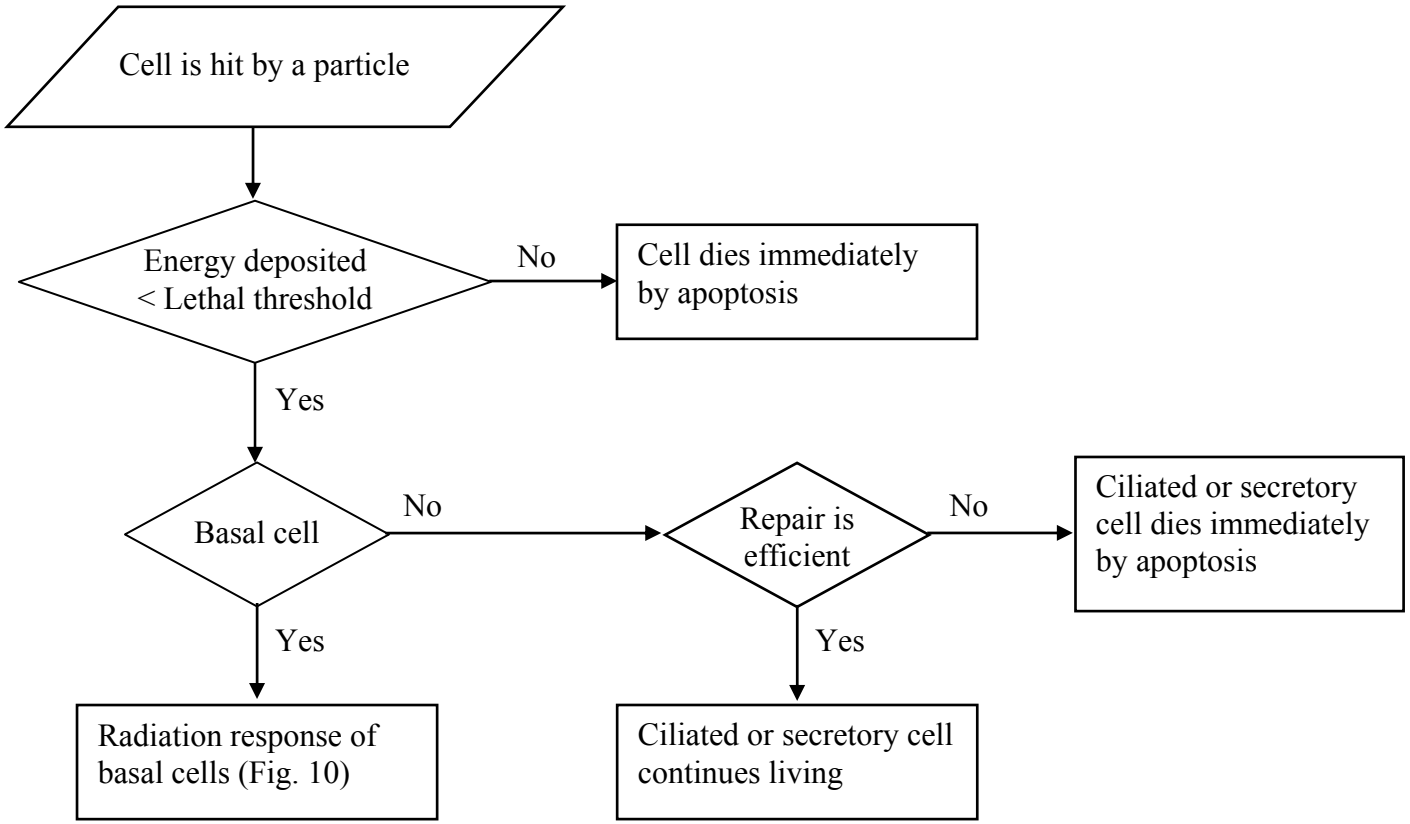


**FIG. 9.** Radiation response of bronchiolar epithelial cells.

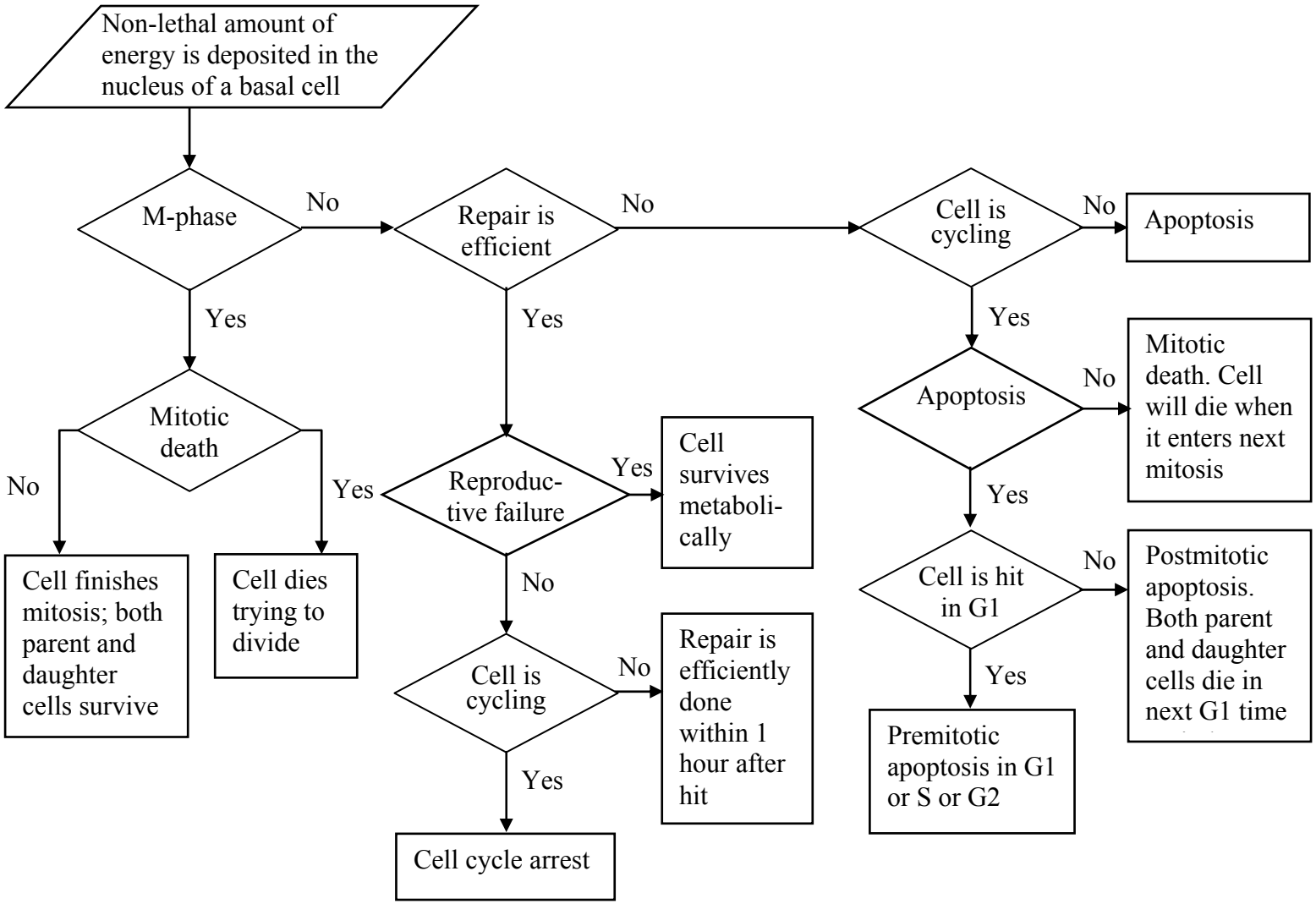


**FIG. 10.** Radiation response of basal cells.

damage. The model calculates the time needed for repair based on the number of single-strand breaks (SSB) and double-strand breaks (DSB) produced in the cellular DNA. The yield of DNA breaks produced by radiation is reported to be about 40 DSBs and about 1000 SSBs per cell per Gy (*75, 76*). The number of the SSBs and DSBs produced in the cellular DNA is estimated from the specific energy deposited in the cell nucleus.

The repair times for the SSBs and DSBs were estimated from the data reported by others. Banath *et al.* studied X-ray induced DNA strand-break rejoining kinetics in human peripheral white blood cells (*77*). They reported that about 50% of the single strand breaks rejoined within first 30 minutes after the exposure to radiation. The single strand break rejoining halftime for the slow component was estimated to be 1.3 hours. Metzger and Iliakis studied the kinetics of the DNA DSB repair in CHO cells exposed to 50 Gy X-rays (*78*). They reported that kinetics of DSB rejoining was biphasic. About 40% of the breaks were repaired by the slow component with repair halftime 1 – 1.5 h; the remaining 60% of the DSBs were repaired by the fast component with rejoining halftime 7 – 14 min. Mozdarani and Bryant reported that half-time for rejoining of DBS induced by X-rays in normal human fibroblasts was 2.7 h, which is similar to the halftime obtained for Ehrlich ascites tumour cells by Blocher: $2.5 \pm 0.7$ h (*79, 80*). Olive and Banath reported much shorter rejoining halftimes for V79 Chinese hamster lung fibroblasts exposed to X-rays: 4.9 min and 13.3 min for SSBs and DSBs, respectively (*summarized in 81*). Foray *et al.* found that double strand breaks induced by α particles were repaired more slowly than those induced by γ-radiation (*82*). Blocher studied radiation-induced double strand breaks in Ehrlich ascites tumor cells.

He reported that after α-particle irradiation the repair halftime was 6 ± 2 h, while for X-rays the repair halftime was 2.5 ± 0.7 h (*80*).

Using these data, it is possible to estimate the maximum repair time for a hit basal cell. A basal cell has a non-zero survival probability if the energy deposited in the cell nucleus is less than the lethal threshold (defined above). Thus, for a basal cell with a nuclear diameter equal to 8 μm, the maximum specific energy deposited in the nucleus (at which the cell may survive) does not exceed 0.12 Gy. For this specific energy value, the estimated number of SSBs and DSBs in the cellular DNA is 120 and 4.8, accordingly. Now, the repair time can be calculated from Equation 8. It is assumed that the repair is complete when the remaining number of breaks is less than one ($N(t) \leq$ 0.5 in Eq. 8).

$$N(t) = N_0 \exp(-t \ln(2) / T_{1/2}) \tag{8}$$

where $N_0$ represents the initial number of breaks,

$N(t)$ represents the number of breaks at time t,

$T_{1/2}$ equals the repair half-time.

The maximum DNA repair times for basal cells (nucleus diameter is 8 μm) were calculated and are summarized in Table 3. Since the estimated repair times for SSBs and DSBs induced by X-ray exposure vary significantly for different input parameters (rejoining halftime), the model uses the most conservative rejoining halftime values for calculation of the repair time. Thus, the progression of the basal cell through the cell cycle will be delayed for the time needed to eliminate the damage; the duration of the current cell-cycle phase will be increased by the repair time.

**TABLE 3**
**DNA single-strand and double-strand breaks rejoining kinetics**

| | DNA breaks rejoining halftime, halftime (% breaks repaired) | Estimated repair time, h |
|---|---|---|
| X-rays | 0.5 h (50%), 1.3 h (50%) [a] | 12.4[b] |
| SSBs | 4.9 min (100%) [c] | 0.6 |
| X-rays | 1.25 (40%), 10.5 min (60%) (averaged data)[d] | 2.9[b] |
| DSBs | 13.3 min (100%) [c] | 0.7 |
| | 2.5 h (100%) [e] | 8.2 |
| α-particles DSBs[f] | 6 h (100%) [e] | 19.6 |

[a] - Banath *et al.* (*77*).
[b] - Total SSB repair time is the sum of the repair times for slow and fast components.
[c] - P. L. Olive (*81*).
[d] - Metzger and Iliakis (*78*).
[e] - Mozdarani and Bryant (*79*), Blocher (*80*).
[f] - The SSB:DSB ratio is much less than 1000:40 for α particles (*83*). Since the double-strand breaks produced by α particles have much longer rejoining halftime, the repair time is calculated only for DSBs.

*Repair.* The sensitivity of the cells to radiation varies through the cell cycle: cells in late S-phase are most radiation-resistant, cells in early S-phase and $G_1$-phase show intermediate sensitivity to radiation, while cells in $G_2$/M are found to be the most radio-sensitive (*84, 85*). To approximate the effectiveness of the repair for basal cells in different cell cycle phases, the data on single-cell survival following exposure to X rays were adopted from Sinclair (*86*) and analytical expression were obtained:

$$P_\gamma(D, G_1) = \exp(-0.32D - 0.032D^2) \quad (9)$$

$$P_\gamma(D, S_{early}) = \exp(-0.19D - 0.025D^2) \quad (10)$$

$$P_{\gamma}(D, S_{late}) = \exp(-0.045D - 0.022D^2) \quad (11)$$

$$P_{\gamma}(D, G_2) = \exp(-0.75D) \quad (12)$$

where $D$ is the dose to the cell nucleus.

For exposure to α-particles, the average value of the RBE for α-particles adopted from Thomas *et al*. was used to calculate the approximate repair probabilities for different cell cycle phases from the survival data for the X-ray exposure (*86, 87*):

$$P_{\alpha}(D, ccp) = P_{\gamma}(D, ccp) / RBE_{\alpha} \quad (13)$$

where $RBE_{\alpha}$ is the relative biological effectiveness of α-particles, $RBE_{\alpha} = 10$,

*ccp* is the cell cycle phase ($G_1$, S, or $G_2$),

$D$ is the dose to the cell nucleus.

*Reproductive failure.* A basal cell may lose its reproductive capacity following radiation exposure. In this case, the cell survives metabolically, but is no longer able to divide. A resting basal cell with zero or non-zero proliferative potential or an actively cycling cell is assigned a $G_0$-phase of the cell cycle and declared a non-reproductive cell. When the bronchiolar epithelium suffers significant cell loss following irradiation, the reproductive basal cells (including cells with zero proliferative potential) may be forced to enter cell cycle and divide in order to replenish the injured tissue. However, non-reproductive basal cells will not be capable of re-entering cell cycle. The model assumes that a basal cell will lose its reproductive capacity if the energy deposited in the cell nucleus is greater than half of the lethal threshold energy.

*Mitotic death.* If an ionizing particle traverses a cycling basal cell in M-phase of the cell cycle and the amount of energy deposited in the nucleus is not lethal, the basal cell may undergo mitotic death. In this case the basal cell continues through its cell

cycle toward mitosis and dies trying to finish mitosis. The model assumes that a cell hit in M-phase of the cell cycle dies by mitotic death if the energy deposited in the cell nucleus is greater than half of the lethal threshold energy.

*Radiation-induced apoptosis.* When a basal cell is hit in $G_1$-phase of the cell cycle, premitotic apoptosis may be induced and the cell will die before it reaches mitosis (in $G_1$-, S-, or $G_2$-phase). If the cell is hit in either the S-phase or $G_2$-phase, postmitotic apoptosis is triggered: both parent and daughter cell die within time period equal to the default value of the $G_1$-phase duration. The model assumes that, for a basal cell hit in $G_1$-, S-, or $G_2$-phase of the cell cycle, the probability of apoptosis induction is equal to the probability of mitotic death.

# CHAPTER IV

## RESULTS AND DISCUSSION

A combined model of tissue kinetics and radiation response of human bronchiolar epithelium has been developed. The model allows the simulation of the epithelial tissue kinetics and radiation exposure in four dimensions: three spatial dimensions and a temporal dimension. The population of the construct starts with "seeding" basal stem cells in the basal grid. Stem cells are randomly assigned the positions in the cell cycle with due regard for the percentage of cells in each cell-cycle phase. The bronchiolar epithelium grows during twenty simulated days, after that the epithelial tissue is built and virtual experiments can be run (Fig. 11, 12).

The model allows the simulation of the bronchiolar tissue kinetics for long periods. The vital activity of the normal epithelium has been modeled for one year for two bronchiolar segments of different size: a whole bronchiole (generation 14) and a quarter of the bronchiole. The data on tissue kinetics has been collected and analyzed. The average percentage of the basal cells in each cell-cycle phase, average secretory to ciliated cells ratio, percentage of vacant positions, and the apoptotic indices have been calculated. The data is summarized in Tables 4 and 5. Default parameters for the duration of the basal cell-cycle phases in normal tissue are listed in Table 6. Comparison of the data obtained for the whole bronchiole to the data obtained for the quarter segment of the bronchiole (Tables 4 and 5) indicates that it is possible to use a bronchiolar segment in the simulation. The difference between numbers of basal cells in different phases of the cell cycle does not exceed 0.2 %. The difference between the average ratios of secretory to ciliated cells is negligible. Utilization of a smaller

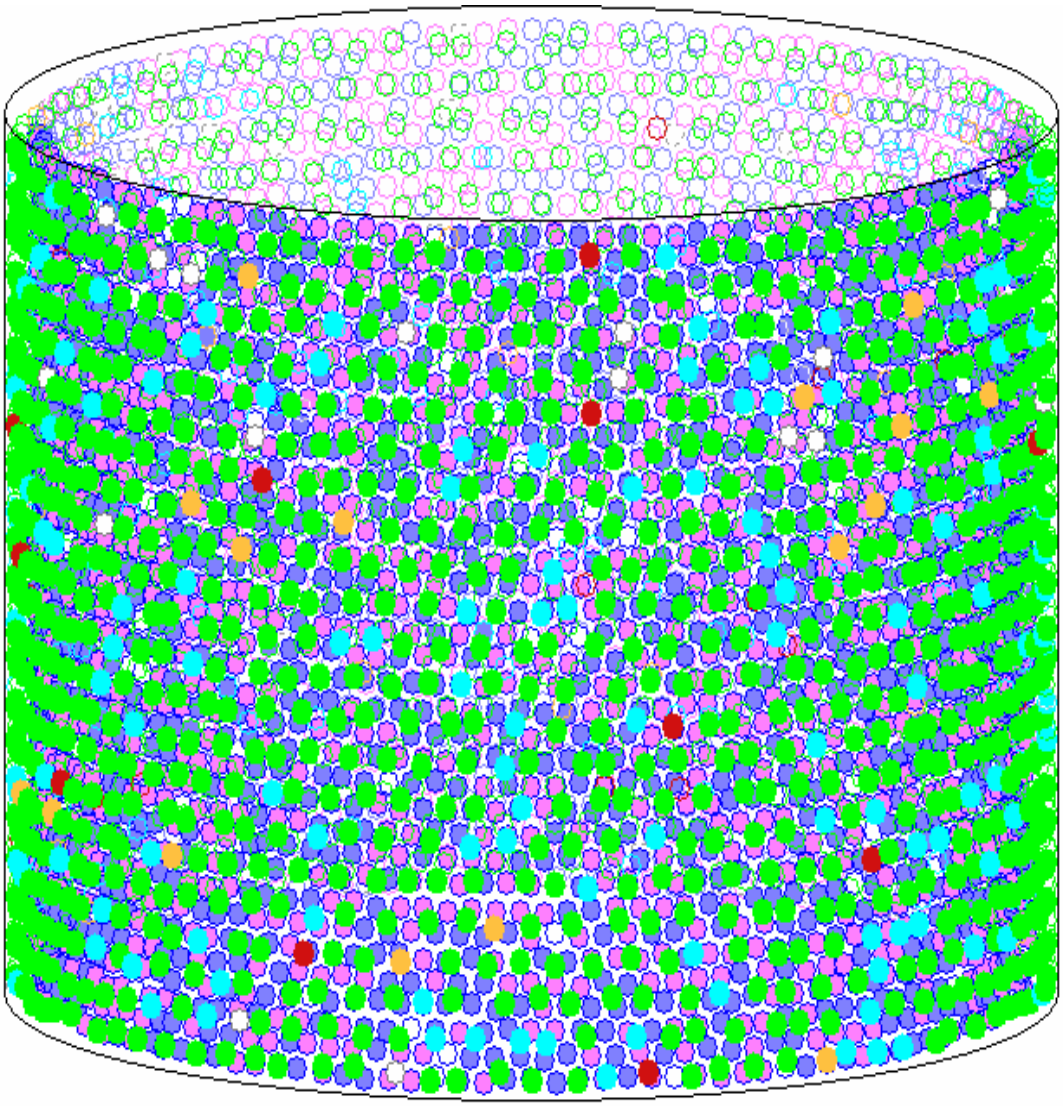

**FIG. 11.** Populated bronchiolar construct. Positions of the cells are marked with circles: green, cyan, orange, and red circles mark basal cells in G0/G1, S, G2, and M phases of the cell cycle, accordingly; blue and pink circles mark secretory and ciliated cells, accordingly.

bronchiole segment leads to a very significant reduction in the simulation time necessary for the calculations.

The epithelium of the pseudo bronchiole (quarter segment) contains up to 1,892 basal and up to 4,480 ciliated and secretory cells. This corresponds to cell density of approximately 784,600 cell/cm$^2$, which is in the range of reported values (*34, 36*). The

**TABLE 4**
**Percentage of basal cells in different cell-cycle phases, percentage of vacant positions in the basal cell grid, and apoptotic index for basal cells for a whole and a quarter segment of a generation-14 bronchiole**

| | $G_0/G_1$, % | S, % | $G_2$, % | M, % | Vacant, % | AI, % |
|---|---|---|---|---|---|---|
| Whole bronchiole, generation 14 | 81.83 | 10.38 | 5.19 | 2.60 | 1.87 | 0.18 |
| Quarter of a bronchiole, generation 14 | 81.67 | 10.47 | 5.24 | 2.62 | 2.11 | 0.20 |
| Absolute difference | 0.16 | 0.09 | 0.05 | 0.02 | 0.24 | 0.02 |

**TABLE 5**
**Average secretory to ciliated cell ratio, percentage of vacant positions in the secretory and ciliated cells grid, and apoptotic index for secretory and ciliated cells for a whole and a quarter segment of a generation-14 bronchiole**

| | Secretory to ciliated cell ratio | Vacant, % | AI, % |
|---|---|---|---|
| Whole bronchiole, generation 14 | 0.99 | 2.85 | 0.38 |
| Quarter of a bronchiole, generation 14 | 1.00 | 3.33 | 0.38 |
| Absolute difference | 0.01 | 0.48 | 0.00 |

**TABLE 6**
**Duration of the cell-cycle phases for basal cells in normal tissue**

| | $G_1$, h | S, h | $G_2$, h | M, h |
|---|---|---|---|---|
| Basal non-stem cells | 24 ± 47 | 8 | 4 | 2 |
| Basal stem cells | 48 ± 71 | 8 | 4 | 2 |

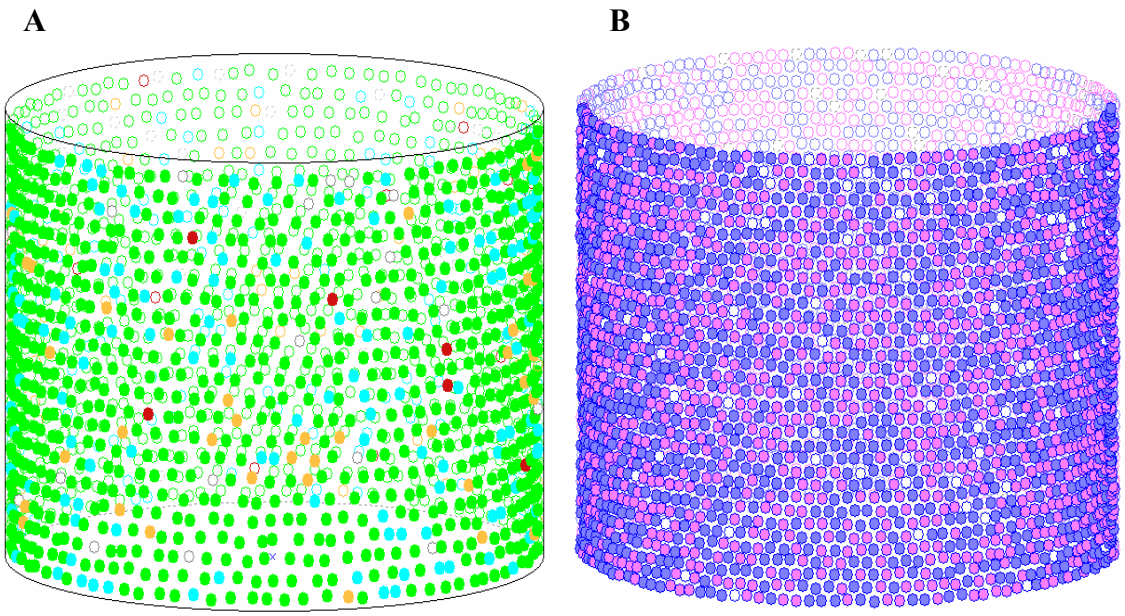


**FIG. 12.** Basal and secretory/ciliated layers in the populated bronchiolar construct. Panel A: Basal cell layer: Green, cyan, orange, and red circles mark basal cells in G0/G1, S, G2, and M phases of the cell cycle, accordingly. Panel B: Secretory (blue) and ciliated (pink) cells lining the surface of the bronchiolar lumen.

basal cell to ciliated and secretory cells ratio is 3:7. The ratio of secretory to ciliated cells calculated by the model is about 1:1, which also is in agreement with the experimental data. The secretory and ciliated cells fill the bronchiole surface in random patches (Fig. 12B). This pattern reflects the batches that have been reported from mammalian samples.

The model has been modified to simulate the circadian oscillations of the fraction of basal cells in different cell-cycle phases. Mitotic activity of the basal cells varies from 0.5% at noon to 4.5% at night, approximately. Basal cells synthesize DNA more actively during the daytime, 16% maximum; DNA synthesis slows to a minimum 4.25 % of the basal cells, at night (Fig. 13). These levels of activity correspond to the experimental results summarized by Brown (*56*).

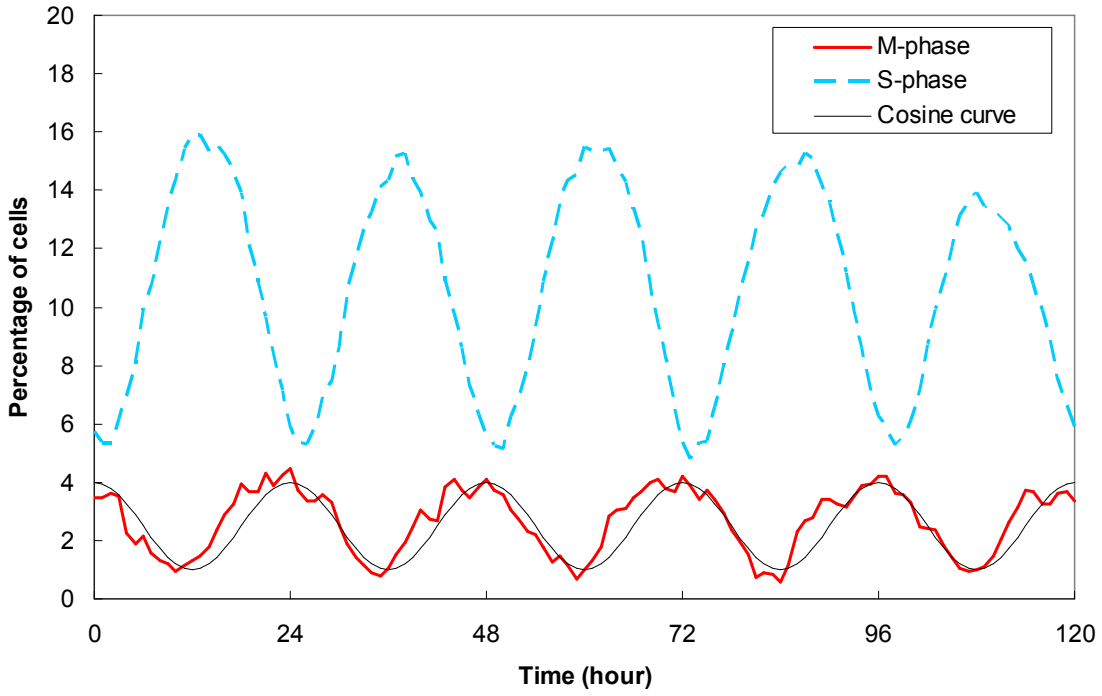


**FIG. 13.** Circadian variation of the percentage of basal cells in M-phase and S-phase of the cell cycle in normal bronchiolar epithelium. *a=0.8*, *b=1* – parameters in the Eq. (1).

The mean turnover time for the bronchiolar epithelial tissue has been calculated 30.2 ± 0.1 days (n=3). The average turnover time reported for the lung epithelial tissues is about 30 days (*88*). The values of the mitotic and labeling indices calculated by the model for normal tissue correspond to the experimental data reported by others. The average mitotic index calculated by the model for normal epithelial tissue is 0.78 %. Bolduc and Reid (*89*) reported the value of the mitotic index for the distal airway in the normal rat lung 0.7%. For normal human airway epithelium, Boers *et al*. reported that proliferation fraction was 0.87% (*34*). The average percentage of the basal cells synthesizing DNA per hour (labeling index, LI) calculated by the model is about 3.1%. This value is close to the data reported by Fabrikant for cells in human bronchus: LI = 4.6% (*44*). In the model, stem cell lifespan ranges from 30 to 60 days. The lifespan for

non-stem basal cells varies from 1 to 50 days. The average lifespan of a non-stem cell is 12 days. Most of the non-stem cells stay alive up to three weeks, which corresponds to the value reported by Spencer and Shorter (*90*). The number of basal cells that stay alive for more than 21 day is less than 1%.

Monte Carlo subroutines have been developed to simulate exposure of the bronchiolar epithelium to α-particles. To see whether the damaged epithelial cells accumulate in the bronchiolar tissue over time, the exposure to α-particles emitted by the radon daughters Po-214 and Po-218, was simulated for 0.5, 1, 2, 3, 4, and 5 year periods. The activity of Po-214 and Po-218 resulting from an exposure of 1 WL (working level) with atmospheric characteristics typical of mines was adopted from Harley (*91*). The values for activity of Po-214 and Po-218 corresponding to the exposure of 1 WL were estimated as 11.7 and 38.7 mBq/cm$^2$, accordingly.

When no radiation exposure is simulated, the majority of the basal cells die by apoptosis due to cell aging (97.92%). Only a small fraction of the basal cells die by apoptosis triggered by a faulty event in the cell (2.08%). Radiation exposure to 1 WL of Po-214 and Po-218 leads to the redistribution of the types of deaths experienced by the basal cells. The number of basal cells dying because of aging or faulty event decreases from 100% to 97.94%. About 2.06% of the basal cell deaths are induced by radiation. Most of the cells damaged by radiation die immediately by apoptosis. The number of basal cells undergoing delayed premitotic or postmitotic apoptosis or mitotic death is less than 0.01% of the dying basal cells.

The model calculates the total number of α-particle traversals for the epithelial cells over the simulated time period. For the radiation exposure at 1 WL, the average

number of basal cells traversed by an α-particle per day is two (here, the average is calculated as the total number of hit cells divided by the number of days in the simulated time period), whereas the average number of hit secretory and ciliated cells per day is 6.3. Since the ranges of α-particles emitted by both Po-214 and Po-218 are greater than the thickness of the bronchiolar epithelium, the ratio of hit basal cells to hit secretory and ciliated cells is close to the ratio of these cells in the tissue.

The average tissue turnover time has been calculated for 0.5, 1, 2, 3, 4, and 5-year time periods. Bronchiolar tissue turnover rate under these irradiation conditions does not differ from the mean turnover rate for normal epithelium (Table 7).

To trace the accumulation of the potentially damaged cells (hit cells or cells that are descendants of the hit cells) in the bronchiolar epithelium, the cell histories are stored into a file at the end of simulation. Analysis of cells' histories at times 0.5, 1, 2,

**TABLE 7**
**Epithelial tissue turnover time under normal and irradiation conditions (1 WL exposure to Po-214 and Po-218 α-particles)**

| Mean turnover time[a] (no radiation), day | Average turnover time[b] (radiation exposure of 1 WL: Po-214 and Po-218), day | | | | | |
|---|---|---|---|---|---|---|
| | 0.5 year[c] | 1 year | 2 years | 3 years | 4 years | 5 years |
| 30.2 ± 0.1 | 24.0 ± 5.4 | 31.3 ± 3.2 | 30.3 ± 3.2 | 30.9 ± 3.3 | 30.5 ± 2.8 | 30.4 ± 3.5 |

[a] Mean turnover time ± standard deviation of the mean (calculated for 1 year, n = 3).
[b] Average turnover time ± standard deviation (calculated for 1 run).
[c] Turnover time calculated for half-year simulation differs from other values due to small data sample.

**TABLE 8**
**Current number of potentially damaged basal, secretory and ciliated cells in the bronchiolar tissue (1 WL exposure to Po-214 and Po-218 α-particles)**

| Time period, year | Current number of living cells hit by α-particles during their lifespan | Current number of descendents of the hit cells | Maximum number of hit progenitors in the cell lineage | Total current number of potentially damaged cells |
|---|---|---|---|---|
| Basal cells | | | | |
| 0.5 | 2 | 4 | 8 | 4 |
| 1 | 2 | 2 | 2 | 4 |
| 2 | 2 | 7 | 2 | 7 |
| 3 | 2 | 2 | 2 | 4 |
| 4 | 2 | 3 | 2 | 3 |
| 5 | 1 | 3 | 2 | 3 |
| Ciliated and secretory cells | | | | |
| 0.5 | 3 | 5 | 7 | 8 |
| 1 | 2 | 12 | 4 | 14 |
| 2 | 2 | 4 | 3 | 6 |
| 3 | 3 | 3 | 1 | 6 |
| 4 | 1 | 7 | 2 | 8 |
| 5 | 3 | 0 | 0 | 3 |
| All cells in the bronchiolar tissue | | | | |
| 0.5 | 5 | 9 | 8 | 12 |
| 1 | 4 | 14 | 4 | 18 |
| 2 | 4 | 11 | 3 | 13 |
| 3 | 5 | 5 | 2 | 10 |
| 4 | 3 | 10 | 2 | 11 |
| 5 | 4 | 3 | 2 | 6 |

3, 4, and 5 years is summarized in Table 8. There is no increase in the number of the potentially damaged cells over the 5-year time period. The model also allows the estimation of the average number of living cells that were hit by α-particles during their lifespan (per hour), the average number of descendents of the hit cells (per hour), the average number of hit progenitors in the cell lineage, the maximum number of hit

**TABLE 9**
**Average number of potentially damaged basal, secretory and ciliated cells in the bronchiolar tissue (1 WL exposure to Po-214 and Po-218 α-particles)**

| Time period, year | Average number of living cells hit by α-particles during their lifespan, per hour | Average number of descendents of the hit cells, per hour | Average number of hit progenitors in the cell lineage, per hour | Maximum number of hit progenitors in the cell lineage | Average total number of potentially damaged cells per hour |
|---|---|---|---|---|---|
| Basal cells | | | | | |
| 0.5 | 0.2 | 0.2 | 1.0 | 1 | 0.4 |
| 1 | 1.2 | 1.2 | 0.8 | 1 | 2.4 |
| 2 | 0.4 | 0.4 | 0.4 | 2 | 0.9 |
| 3 | 0.5 | 0.5 | 0.4 | 1 | 1.1 |
| 4 | 0.5 | 0.5 | 0.4 | 2 | 1.1 |
| 5 | 0.4 | 0.4 | 0.3 | 1 | 0.7 |
| Ciliated and secretory cells | | | | | |
| 0.5 | 3.1 | 3.1 | 1.0 | 1 | 6.2 |
| 1 | 2.9 | 2.9 | 0.9 | 1 | 5.8 |
| 2 | 3.5 | 3.5 | 0.9 | 2 | 7.1 |
| 3 | 3.5 | 3.5 | 1.0 | 2 | 7.1 |
| 4 | 3.6 | 3.6 | 1.0 | 2 | 7.2 |
| 5 | 3.6 | 3.6 | 1.0 | 2 | 7.2 |
| All cells in the bronchiolar tissue | | | | | |
| 0.5 | 3.3 | 3.3 | 2.0 | 1 | 6.6 |
| 1 | 4.1 | 4.1 | 1.7 | 1 | 8.2 |
| 2 | 4.0 | 4.0 | 1.3 | 2 | 8.0 |
| 3 | 4.1 | 4.1 | 1.4 | 2 | 8.2 |
| 4 | 4.2 | 4.2 | 1.4 | 2 | 8.3 |
| 5 | 4.0 | 4.0 | 1.3 | 2 | 7.9 |

progenitors in the cell lineage, and the average total number of potentially damaged cells (per hour) (Table 9).

The average numbers of the basal cells in different cell-cycle phases and vacant positions in the basal cell grid, and the average apoptotic index (percentage of dying cells per hour) have been calculated for different periods of time (see Table 10). There

is no significant redistribution of cell numbers between different cell-cycle phases over time. A slight increase is observed in the rate of basal cell proliferation: shorter duration of the $G_0$-phase indicates that basal cells tend to enter the cell cycle faster compared to non-irradiated conditions. A small decrease in density of the basal cells in the tissue is observed under radiation conditions. The apoptotic index for basal cells decreases by a fraction of a percent.

The average secretory to ciliated cells ratios, the average percentage of vacant positions in the ciliated and secretory grid, and the average apoptotic index have been calculated for the same time periods (see Table 11). A small decrease in density of the ciliated and secretory cells in the tissue is observed with irradiation. The average secretory to ciliated cells ratio and the apoptotic index for ciliated and secretory cells do

**TABLE 10**
**Average values for percentage of basal cells in different cell cycle phases, percentage of vacant positions in the basal cell grid, and apoptotic index (AI) for basal cells for 0.5, 1, 2, 3, 4, and 5-year periods for radiation exposure of 1 WL to Po-214 and Po-218 α-particles**

| Time period, year | $G_0$, % | $G_1$, % | S, % | $G_2$, % | M, % | Vacant positions, % | AI, % |
|---|---|---|---|---|---|---|---|
| 0 (no radiation) | 26.44 | 55.08 | 10.56 | 5.28 | 2.64 | 1.99 | 0.19 |
| 0.5 | 25.74 | 55.56 | 10.70 | 5.34 | 2.67 | 2.38 | 0.20 |
| 1 | 25.84 | 55.48 | 10.68 | 5.34 | 2.67 | 2.34 | 0.20 |
| 2 | 25.88 | 55.45 | 10.67 | 5.33 | 2.67 | 2.32 | 0.20 |
| 3 | 25.91 | 55.43 | 10.67 | 5.33 | 2.66 | 2.32 | 0.20 |
| 4 | 25.87 | 55.45 | 10.68 | 5.34 | 2.67 | 2.37 | 0.20 |
| 5 | 25.83 | 55.48 | 10.68 | 5.34 | 2.67 | 2.34 | 0.20 |

not change significantly over time and do not differ from the values obtained without irradiation.

To estimate the impact of different exposure rates on epithelial tissue kinetics, the bronchiole was virtually "irradiated" by Po-214 and Po-218 α-particles for one year at exposure levels of 0.01, 0.05, 0.1, 0.5, 1, 5, 10, 15, and 20 WL equivalents. Higher exposure rates result in the redistribution of the basal cells in the cell-cycle: the proliferation rate increases as the epithelial tissue tries to replenish the cell loss (Fig. 14).

During simulation of the radiation exposure, at each time step, the model checks on the cellular density in the bronchiolar epithelium. When the cell population decreases below the critical threshold, the model adjusts the cell cycle parameters in

**TABLE 11**
**Average values for secretory to ciliated cell ratio, percentage of vacant positions in the secretory and ciliated cells grid, and apoptotic index (AI) for secretory and ciliated cells for 0.5, 1, 2, 3, 4, and 5-year periods for radiation exposure of 1 WL to Po-214 and Po-218 α-particles**

| Time period, year | Secretory to ciliated cell ratio | Vacant positions, % | AI, % |
|---|---|---|---|
| 0 (no radiation) | 1.00 | 3.02 | 0.38 |
| 0.5 | 0.99 | 3.45 | 0.38 |
| 1 | 0.99 | 3.45 | 0.38 |
| 2 | 1.00 | 3.47 | 0.38 |
| 3 | 1.00 | 3.42 | 0.38 |
| 4 | 1.00 | 3.46 | 0.38 |
| 5 | 1.00 | 3.44 | 0.38 |

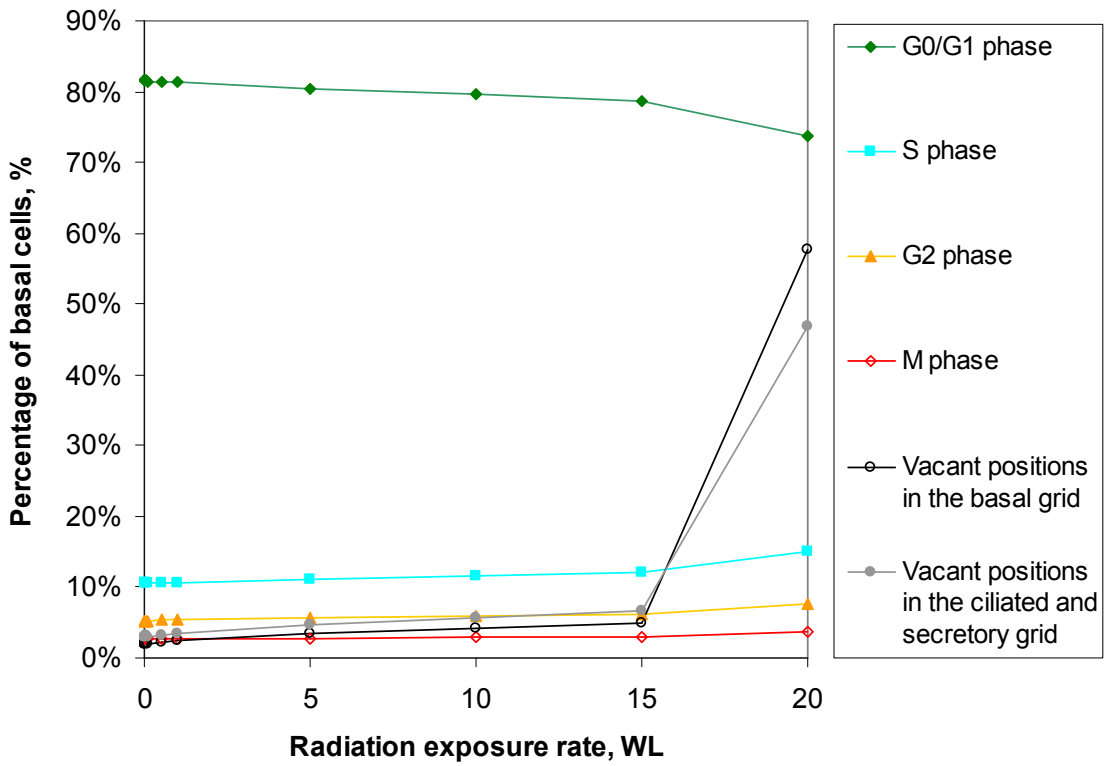


**FIG. 14.** Percentage of basal cells in different cell-cycle phases depending on the radiation exposure rate.

order to maintain the functional integrity of the epithelial tissue (*92, 93*). For the cycling basal cells, the minimum duration of the $G_1$ phase may decrease from 24 to 16 hours for non- stem cells, and from 48 to 24 hours for stem cells. This change in the minimum duration of the $G_1$ phase occurs when the number of vacant positions in the bronchiole construct exceeds 5% of the total cell number. Non-cycling cells with zero proliferative capacity are forced into one more division cycle when the number of vacant positions in the bronchiole construct exceeds 10% of the total cell number. As a result, the average duration of the basal cell $G_1$ phase decreases as the exposure rate increases (Fig. 15), in spite of the cell-cycle delays induced by the radiation.

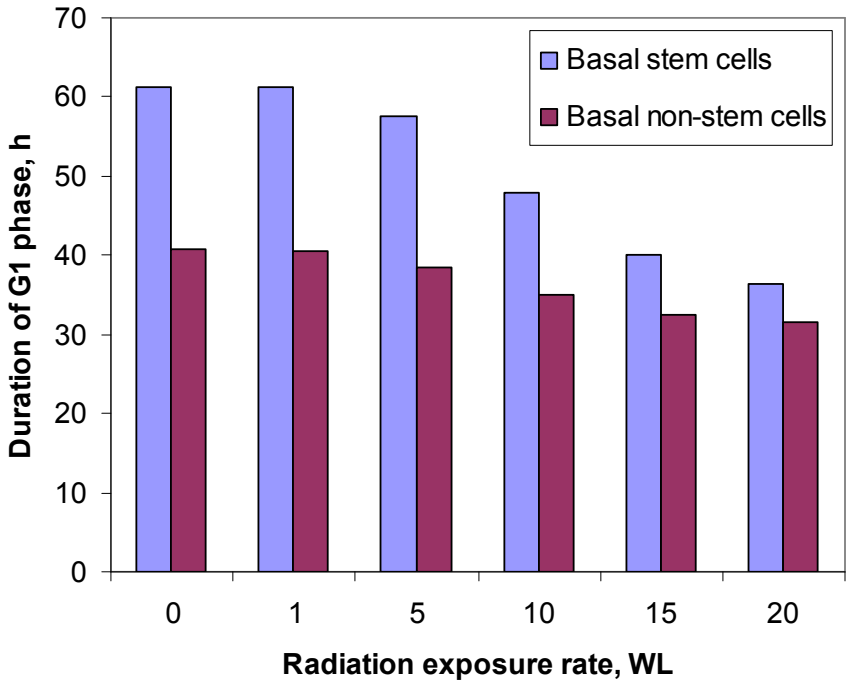


**FIG. 15.** Duration of $G_1$ phase of the cell cycle for stem and non-stem basal cells depending on the radiation exposure rate.

From Figure 14, it can be concluded that there is a threshold between 15 and 20 WL exposure rates where the drastic increase in the number of vacant positions in the bronchiolar construct indicates that the basal cells cannot replenish cell loss. Thus, under the exposure rate more than 15 WL equivalents, the bronchiole will die in less than one year.

The average duration of the cell-cycle delay in $G_1$, S, and $G_2$ phases varies from 7 to 10 hours (Fig. 16). The number of basal cells delayed in the cell-cycle progression is small for 1 WL exposure rate due to small data sample. The data for 20 WL exposure rate is not representative, since almost half of the epithelial cells have died within first two months of the exposure. Therefore, the data points for 1 and 20 WL exposure rates were ignored. Now, the following trends of change in the cell-cycle delay induced in

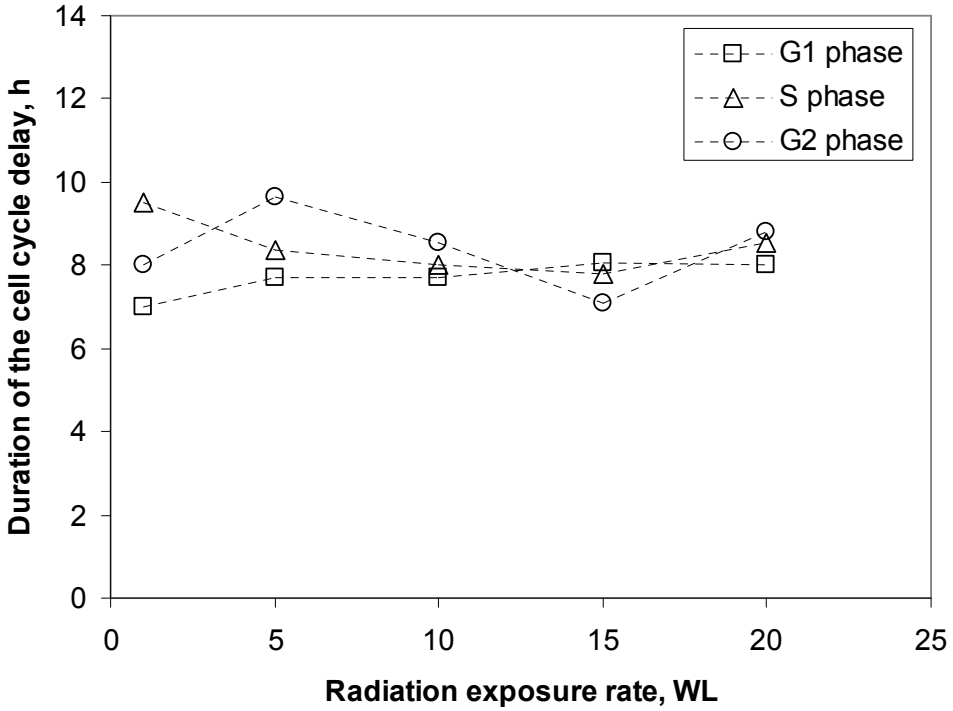


**FIG. 16.** The average duration of the cell-cycle delay in $G_1$, S, and $G_2$ phases of the basal cell cycle depending on the radiation exposure rate.

different phases can be observed: the duration of the $G_1$-phase delay increases, and the duration of both S-phase and $G_2$-phase decrease with the increasing exposure rate (Fig. 16).

The average turnover time of the bronchiolar epithelial tissue decreases with increasing exposure rate (Fig. 17). The data point for 20 WL exposure rate is discarded due to small data sample. The plateau-like region between 5 and 10 WL exposure rates can be explained by the increased influx of the basal cells into the cell cycle (cells live longer) or by the induction of cell-cycle delays. However, for exposure rates higher than 10 WL, the rate of cell killing increases and the epithelial tissue fails to produce new cells in proper time and the average turnover time continues decreasing.

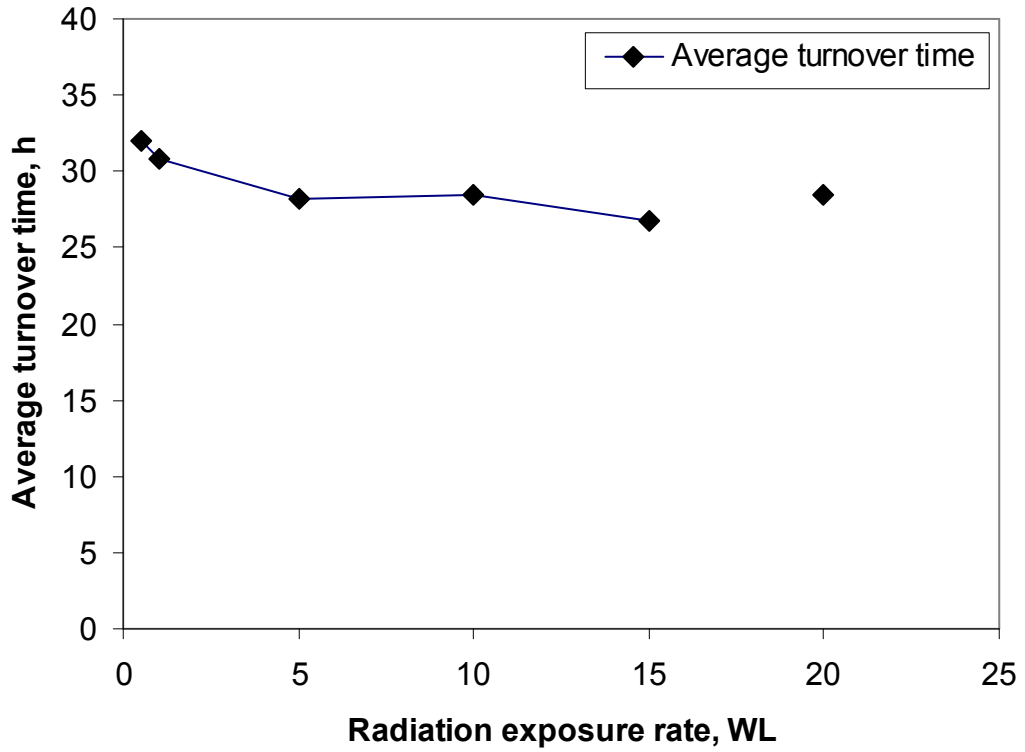


**FIG. 17.** The average turnover time of the bronchiolar epithelial tissue depending on the radiation exposure rate (exposure to Po-214 and Po-218 α-particles).

The percentage of cells dying after being hit by an α-particle increases with increasing exposure rate (Fig. 18). Most of the cells traversed by α-particles die immediately: the delayed apoptosis and mitotic death account only for less than 0.1% of all basal cell deaths. The percentage of the hit cells in the tissue increases lineally from 0.002% at the 0.01 WL exposure rate to 1.75% at 15 the WL exposure rate.

The values of the specific energy deposited by α-particles to the nuclei of the epithelial cells were calculated. The average specific energy deposited by α-particles to the basal cell nucleus is 35.8 ± 0.3 cGy. The average specific energy deposited by α-particles to the nucleus of secretory or ciliated cell is 21.3 ± 0.1 cGy. These values are

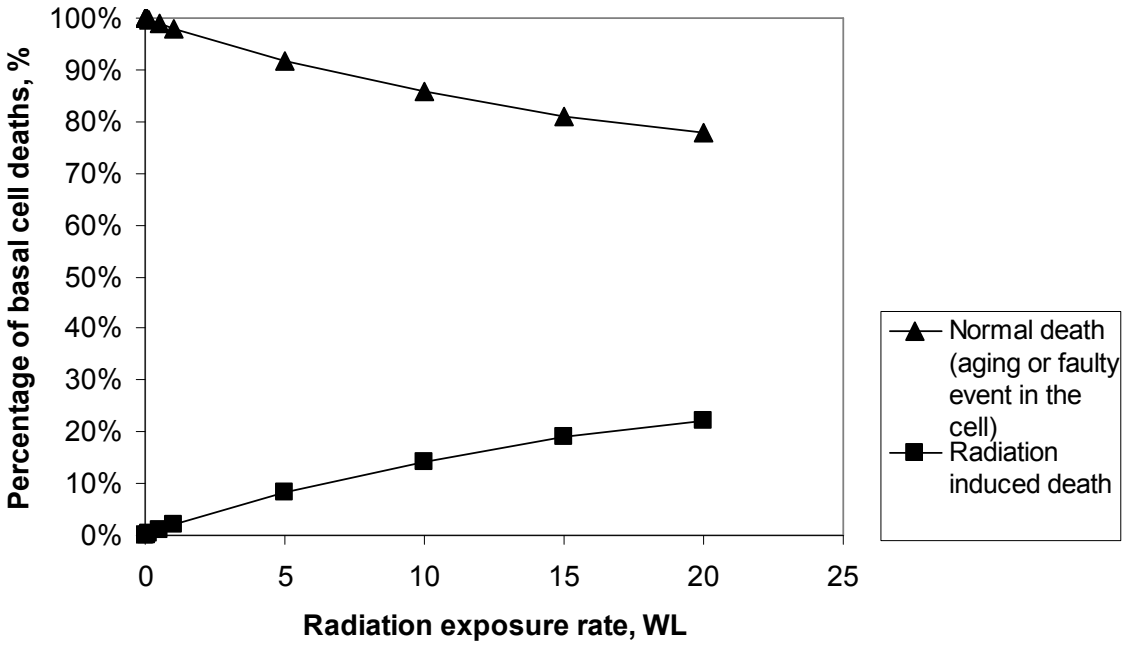


**FIG. 18.** Percentage of the basal cell deaths depending on the radiation exposure rate.

in good agreement with specific energies calculated by Nikezic and Yu for the cell nuclei in sensitive layers of the human respiratory tract (*22*).

The Geant4 software package has been used to model the exposure of the bronchiolar epithelium to low-LET radiations (photons and β-particles). To see whether the bronchiolar epithelial cells suffer damage from internally deposited β-particle emitters, the exposure to β-particles has been simulated for one year period. The daughter products of Rn-222 include Pb-214 and Bi-214 that are β- and γ-emitters. The average energies of β-particles emitted by these radio-nuclides vary from 0.02 to 1.27 MeV. The range of a 0.02 MeV β-particle in tissue is about 10 μm, which is shorter than the distance from the mucociliary layer to the basal cell layer. Therefore, the exposure of the bronchiole was modeled for β-particles with energies 0.05, 0.1, 0.2, 0.5, 1.0, and 1.25 MeV. The activity of β-particles resulting from an exposure of 1 WL with atmospheric characteristics typical of mines was adopted from Harley (*91*).

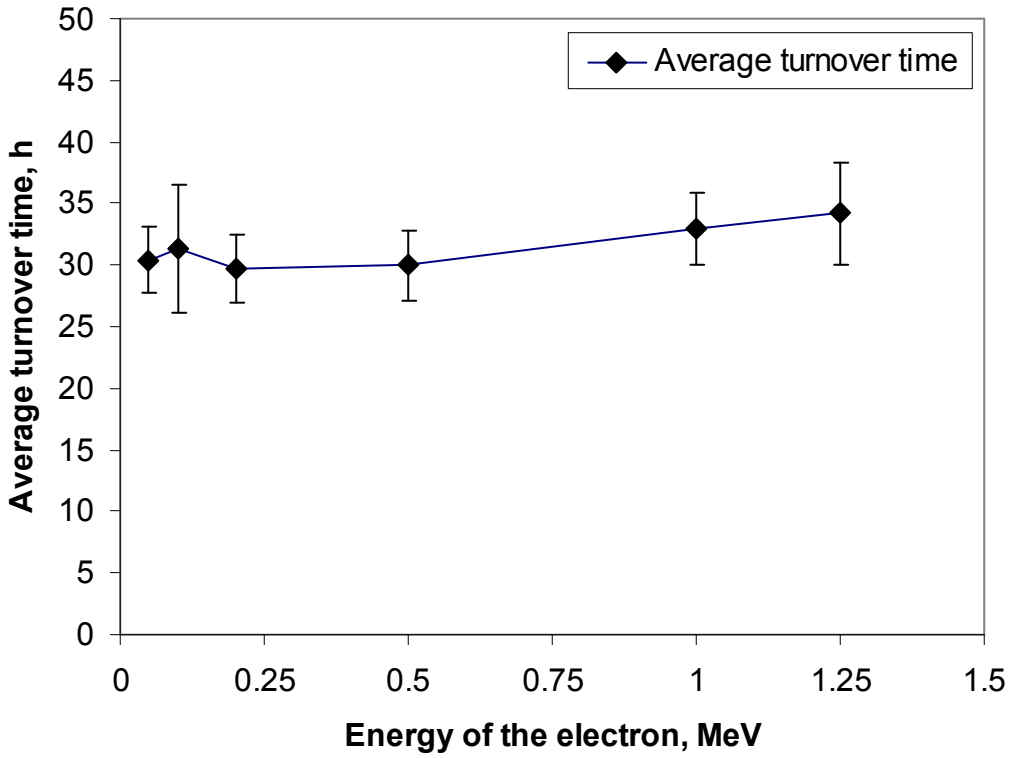


**FIG. 19.** The average turnover time of the bronchiolar epithelial tissue depending on the radiation exposure rate (exposure to Pb-214 and Bi-214 β-particles).

Low level radiation exposure to β-particles does not lead to the redistribution of the death types for the basal cells, since there is no cell killing. The model calculates the total number of β-particle traversals for the epithelial cells over the simulated time period. For the radiation exposure at 1 WL, the average number of basal cells traversed by a β-particle per day varies from 0.4 to 1.0 cells for 0.05 and 0.1 MeV β-particles, accordingly. The average number of cell traversals per day for the secretory and ciliated cells varies from 0.3 to 0.8 cells for 0.5 and 0.1 MeV β-particles, accordingly.

**TABLE 12**
**Average number of potentially damaged basal, secretory and ciliated cells in the bronchiolar tissue due to 1 WL one-year exposure to β-particles**

| Energy of β-particle, MeV | Average number of living cells hit by β-particles during their lifespan, per hour | Average number of descendents of the hit cells, per hour | Average number of hit progenitors in the cell lineage, per hour | Maximum number of hit progenitors in the cell lineage | Average total number of potentially damaged cells per hour |
|---|---|---|---|---|---|
| Basal cells | | | | | |
| 0.05 | 7.4 | 44.0 | 2.8 | 9 | 46.8 |
| 0.10 | 21.2 | 167.6 | 1.8 | 14 | 175.1 |
| 0.20 | 17.7 | 167.7 | 1.6 | 11 | 173.5 |
| 0.50 | 11.0 | 105.0 | 1.8 | 9 | 108.7 |
| 1.00 | 11.3 | 71.0 | 1.8 | 10 | 74.8 |
| 1.25 | 12.7 | 111.3 | 1.7 | 8 | 116.1 |
| Ciliated and secretory cells | | | | | |
| 0.05 | 4.5 | 108.8 | 2.7 | 10 | 113.0 |
| 0.10 | 4.8 | 396.4 | 1.8 | 15 | 400.0 |
| 0.20 | 3.5 | 389.1 | 1.7 | 12 | 392.1 |
| 0.50 | 1.9 | 247.0 | 1.8 | 10 | 248.7 |
| 1.00 | 2.4 | 170.3 | 1.9 | 10 | 172.4 |
| 1.25 | 2.6 | 264.0 | 1.7 | 9 | 266.3 |
| All cells in the bronchiolar tissue | | | | | |
| 0.05 | 11.9 | 152.7 | 5.5 | 19.0 | 159.8 |
| 0.10 | 26.0 | 564.0 | 3.6 | 29.0 | 575.1 |
| 0.20 | 21.3 | 556.8 | 3.3 | 23.0 | 565.6 |
| 0.50 | 12.9 | 352.0 | 3.7 | 19.0 | 357.4 |
| 1.00 | 13.7 | 241.2 | 3.8 | 20.0 | 247.1 |
| 1.25 | 15.3 | 375.2 | 3.4 | 17.0 | 382.4 |

The average tissue turnover time has been calculated for β-particles with different kinetic energies. The turnover rate of the bronchiolar epithelium increases slightly with increasing particle energy (Fig. 19). This increase is probably caused by the induction of the delays in the progression of the basal cells through the cell cycle.

The average duration of the cell-cycle delay in $G_1$, S, and $G_2$ phases varies from 1 to 4.5 hours.

The average number of living cells hit by β-particles during their lifespan (per hour), the average number of descendents of the hit cells (per hour), the average number of hit progenitors in the cell lineage, the maximum number of hit progenitors in the cell lineage, and the average total number of potentially damaged cells (per hour) were calculated and summarized in Table 12. The average total number of potentially damaged epithelial cells produced by β-particles with different kinetic energies is about 380 cell/hour, which is much greater compared to the value calculated for α-particles (8.2 cells/hour for one year exposure, see Table 9). However, the average specific energy deposited by α-particles to the cell nucleus is about 200 times larger than the average specific energy deposited by β-particles. Under this irradiation conditions, all epithelial cells traversed by β-particles successfully repair the damage. The actual damage produced to the cells by β-particles is negligible compared to the damage produced by α-particles.

The average energies of γ-particles emitted by Pb-214 and Bi-214 radio-nuclides vary from 0.01 to 3.3 MeV. The radiation exposure to γ-particles has been simulated for energies 0.300, 0.600, 1.120, and 1.765 MeV. These energy values were picked based on the relative intensity of the γ-ray emission. It was found that no energy deposition have occurred in the nuclei of the cells of the bronchiolar epithelial layer. Hence, for the purposes of assessment of radiation damage to the cells of the bronchiolar epithelium, the exposure to internally deposited γ-emitters can be ignored.

# CHAPTER V

# CONCLUSIONS

The combined model of tissue kinetics and radiation response of human bronchiolar epithelium has been developed. The novelty of the approach used was to build the bronchiolar epithelial tissue construct from bottom up, cell by cell, taking into account geometric and morphometric parameters of human bronchioles and cells populating the bronchiolar epithelium. The model describes the bronchiolar epithelial tissue kinetics and allows simulating the long term exposure to ionizing radiation. Validation of the model has been carried out by comparison the calculated values and the experimental data obtained by others. The model output results for the bronchiolar tissue kinetics are in good agreement with the reported experimental values. The model can be used to trace the accumulation of damage in the cells of the bronchiolar epithelium following exposure to different types of ionizing radiation.

# REFERENCES


1. E. G. Luebeck and W. D. Hazelton, Multistage carcinogenesis and radiation. *J. Radiol. Prot*. **22**, A43-49 (2002).
2. J. S. Rhim, Neoplastic transformation of human epithelial cells in vitro. *Anticancer Res.* **9**, 1345-1365 (1989).
3. J. S. Rhim, J. H. Yoo, J. H. Park, P. Thraves, Z. Salehi and A. Dritschilo, Evidence for the multistep nature of in vitro human epithelial cell carcinogenesis. *Cancer Res*. **50**, 5653S-5657S (1990).
4. K. Suzuki, Multistep nature of X-ray-induced neoplastic transformation in mammalian cells: Genetic alterations and instability. *J. Radiat. Res. (Tokyo)* **38**, 55-63 (1997).
5. B. Vogelstein and K. W. Kinzler, The multistep nature of cancer. *Trends Genet*. **9**, 138-141 (1993).
6. J. B. Little, Genomic instability and radiation. *J. Radiol. Prot.* **23**, 173-181 (2003).
7. L. E. Smith, S. Nagar, G. J. Kim and W. F. Morgan, Radiation-induced genomic instability: Radiation quality and dose response. *Health Phys.* **85**, 23-29 (2003).
8. W. F. Morgan, Non-targeted and delayed effects of exposure to ionizing radiation: I. Radiation-induced genomic instability and bystander effects in vitro. *Radiat. Res.* **159**, 567-580 (2003).
9. W. F. Morgan, Non-targeted and delayed effects of exposure to ionizing radiation: II. Radiation-induced genomic instability and bystander effects in vivo, clastogenic factors and transgenerational effects. *Radiat. Res.* **159**, 581-596 (2003).

10. E. I. Azzam and J. B. Little, The radiation-induced bystander effect: Evidence and significance. *Hum. Exp. Toxicol*. **23**, 61-65 (2004).

11. E. J. Hall, The bystander effect. *Health Phys.* **85**, 31-35 (2003).

12. K. M. Prise, M. Folkard and B. D. Michael, A review of the bystander effect and its implications for low-dose exposure. *Radiat. Prot. Dosimetry* **104**, 347-355 (2003).

13. D. J. Brenner, R. Doll, D. T. Goodhead, E. J. Hall, C. E. Land, J. B. Little, J. H. Lubin, D. L. Preston, R. J. Preston, J. S. Puskin, E. Ron, R. K. Sachs, J. M. Samet, R. B. Setlow and M. Zaider, Cancer risks attributable to low doses of ionizing radiation: Assessing what we really know. *Proc. Natl. Acad. Sci. USA* **100**, 13761-13766 (2003).

14. M. H. Barcellos-Hoff, It takes a tissue to make a tumor: Epigenetics, cancer and the microenvironment. *J. Mammary Gland Biol. Neoplasia* **6**, 213-221 (2001).

15. R. C. Miller, C. R. Geard, M. J. Geard and E. J. Hall, Cell-cycle-dependent radiation-induced oncogenic transformation of C3H 10T1/2 cells. *Radiat. Res*. **130**, 129-133 (1992).

16. K. Konig and H. Baisch, DNA synthesis and cell cycle progression of synchronized L-cells after irradiation in various phases of the cell cycle. *Radiat. Environ. Biophys*. **18**, 257-266 (1980).

17. E. Blakely, P. Chang, L. Lommel, K. Bjornstad, M. Dixon, C. Tobias, K. Kumar and W. F. Blakely, Cell-cycle radiation response: Role of intracellular factors. *Adv. Space Res*.9, 177-186 (1989).

18. ICRP, *Human Respiratory Tract Model for Radiological Protection*. Publication 66, *Annals of the ICRP*, Vol. 24, No. 1-3. Pergamon Press, Oxford, 1994.

19. R. R. Mercer, M. L. Russell and J. D. Crapo, Radon dosimetry based on the depth distribution of nuclei in human and rat lungs. *Health Phys*. **61**, 117-130 (1991).

20. N. H. Harley, P. Chittaporn, O. W. Meyers and E. S. Robbins, A biological model for lung cancer risk from 222Rn exposure. *Environ. Int.* **22** (Suppl.), S977-S984 (1996).

21. D. Nikezic, A. K. Haque and K. N. Yu, Absorbed dose delivered by alpha particles calculated in cylindrical geometry. *J. Environ. Radioact*. **60**, 293-305 (2002).

22. D. Nikezic and K. N. Yu, Distributions of specific energy in sensitive layers of the human respiratory tract. *Radiat. Res*. **157**, 92-98 (2002).

23. D. Nikezic and K. N. Yu, Absorbed fraction of alpha-particles emitted in bifurcation regions of the human tracheo-bronchial tree. *Radiat. Environ. Biophys*. **42**, 49-53 (2003).

24. R. D. Stewart and R. J. Traub, Radiobiological Modeling in Voxel Constructs. In *Proceedings of the MC2000,* An International Conference on Advanced Monte Carlo for Radiation Physics, Particle Transport Simulation and Applications. Lisbon, Portugal, October 23-26, 2000.

25. S. Chauvie, R. Cirio, M. Donetti, F. Marchetto and C. Peroni, A Monte Carlo model for cell-cycle kinetics in charged particle irradiation. *Phys. Med*. **17** (Suppl.), 175-176 (2001).

26. National Research Council, Committee on Health Risks of Exposure to Radon, *Health Effects of Exposure to Radon (BEIR VI)*. National Academy Press, Washington, DC, 1999.

27. Y. Oghiso and Y. Yamada, Immunohistochemical study on cellular origins of rat lung tumors induced by inhalation exposures to plutonium dioxide aerosols as compared to those by X-ray irradiation. *J. Radiat. Res. (Tokyo)* **43**, 301-311 (2002).

28. T. K. Hei, C. Q. Piao, J. C. Willey, S. Thomas and E. J. Hall, Malignant transformation of human bronchial epithelial cells by radon-simulated alpha-particles. *Carcinogenesis* **15**, 431-437 (1994).

29. G. Saccomanno, O. Auerbach, M. Kuschner, N. H. Harley, R. Y. Michels, M. W. Anderson and J. J. Bechtel, A comparison between the localization of lung tumors in uranium miners and in nonminers from 1947 to 1991. *Cancer* **77**, 1278-1283 (1996).

30. T. V. Colby, M. N. Koss and W. D. Travis, *Tumors of the Lower Respiratory Tract,* 3rd ed. Armed Forces Institute of Pathology, Washington, DC, 1995.

31. N. G. Ostrovskaya and J. R. Ford, Modeling the radiation response of respiratory tissue. *Transactions of the American Nuclear Society* **88**, 349 (2003).

32. N. G. Ostrovskaya and J. R. Ford, A combined tissue kinetics and dosimetric model of an airway. *Transactions of the American Nuclear Society* **90**, 57-58 (2004).

33. R. R. Mercer, M. L. Russell, V. L. Roggli and J. D. Crapo, Cell number and distribution in human and rat airways. *Am. J. Respir. Cell. Mol. Biol*. **10**, 613-624 (1994).

34. J. E. Boers, A. W. Ambergen and F. B. Thunnissen, Number and proliferation of basal and parabasal cells in normal human airway epithelium. *Am. J. Respir. Crit. Care Med*. **157**, 2000-2006 (1998).

35. F. Baldwin, A. Hovey, T. McEwen, R. O'Connor, H. Unruh and D. H. Bowden, Surface to nuclear distances in human bronchial epithelium: Relationships to penetration by Rn daughters. *Health Phys*. **60**, 155-162 (1991).

36. M. J. Evans, L. S. Van Winkle, M. V. Fanucchi and C. G. Plopper, Cellular and molecular characteristics of basal cells in airway epithelium. *Exp. Lung Res*. **27**, 401-415 (2001).

37. F. Baldwin, Basal cells in human bronchial epithelium. *Anat. Rec*. **238**, 360-367 (1994).

38. P. Nettesheim, A. M. Jetten, Y. Inayama, A. R. Brody, M. A. George, L. B. Gilmore, T. Gray and G. E. Hook, Pathways of differentiation of airway epithelial cells. *Environ. Health Perspect*. **85**, 317-329 (1990).

39. J. R. Ford and M. Terzaghi-Howe, Basal cells are the progenitors of primary tracheal epithelial cell cultures. *Exp. Cell Res*. **198**, 69-77 (1992).

40. M. L. Zepeda, M. R. Chinoy and J. M. Wilson, Characterization of stem cells in human airway capable of reconstituting a fully differentiated bronchial epithelium. *Somat. Cell. Mol. Genet*. **21**, 61-73 (1995).

41. M. Soderberg, S. Hellstrom, T. Sandstrom, R. Lundgren and A. Bergh, Structural characterization of bronchial mucosal biopsies from healthy volunteers: A light and electron microscopical study. *Eur. Respir. J*. **3**, 261-266 (1990).

42. R. B. Clarke, E. Anderson, A. Howell and C. S. Potten, Regulation of human breast epithelial stem cells. *Cell Prolif.* **36** (Suppl.), 45-58 (2003).

43. C. S. Potten and R. J. Morris, Epithelial stem cells in vivo. *J. Cell. Sci.* **10** (Suppl.), 45-62 (1988).

44. J. I. Fabrikant, The kinetics of cellular proliferation in normal and malignant tissues: A review of methodology and the analysis of cell population kinetics in human tissues. *Am. J. Roentgenol. Radium Ther. Nucl. Med.* **111**, 700-711 (1971).

45. W. R. Otto, Lung stem cells. *Int. J. Exp. Pathol.* **78**, 291-310 (1997).

46. G. M. Cooper, *The Cell: A Molecular Approach*, 2nd ed. ASM Press, Washington, DC, 2000.

47. N. C. Joyce, D. L. Harris and D. M. Mello, Mechanisms of mitotic inhibition in corneal endothelium: Contact inhibition and TGF-beta2. *Invest. Ophthalmol. Vis Sci.* **43**, 2152-2159 (2002).

48. Y. Nakatsuji and R. H. Miller, Density dependent modulation of cell cycle protein expression in astrocytes. *J. Neurosci. Res.* **66**, 487-496 (2001).

49. M. Gos, J. Miloszewska, P. Swoboda, H. Trembacz, J. Skierski and P. Janik, Cellular quiescence induced by contact inhibition or serum withdrawal in C3H10T1/2 cells. *Cell Prolif.* **38**, 107-116 (2005).

50. U. Baumeister, R. Funke, K. Ebnet, H. Vorschmitt, S. Koch and D. Vestweber, Association of Csk to VE-cadherin and inhibition of cell proliferation. *EMBO J.* **24**, 1686-1695 (2005).

51. G. Frentz, U. Moller, P. Holmich and I. J. Christensen, On circadian rhythms in human epidermal cell proliferation. *Acta. Derm. Venereol*. **71**, 85-87 (1991).

52. R. Smaaland, Circadian rhythm of cell division. *Prog. Cell Cycle Res.* **2**, 241-266 (1996).

53. C. S. Potten, D. Booth, N. J. Cragg, G. L. Tudor, J. A. O'Shea, D. Appleton, D. Barthel, T. G. Gerike, F. A. Meineke, M. Loeffler and C. Booth, Cell kinetic studies

in the murine ventral tongue epithelium: Thymidine metabolism studies and circadian rhythm determination. *Cell Prolif.* **35** (Suppl.), 1-15 (2002).

54. L. Rensing and K. Goedeke, Circadian rhythm and cell cycle: Possible entraining mechanisms. *Chronobiologia* **3**, 853-865 (1976).
55. R. M. Das, M. Jain and W. M. Thurlbeck, Circadian rhythm and proliferation of lung alveolar wall cells during postnatal growth in mice. *Am. Rev. Respir. Dis.* **121**, 367-371 (1980).
56. W. R. Brown, A review and mathematical analysis of circadian rhythms in cell proliferation in mouse, rat, and human epidermis. *J. Invest. Dermatol.* **97**, 273-280 (1991).
57. J. F. Kerr, A. H. Wyllie and A. R. Currie, Apoptosis: A basic biological phenomenon with wide-ranging implications in tissue kinetics. *Br. J. Cancer* **26**, 239-257 (1972).
58. A. Shilkaitis, A. Green, V. Steele, R. Lubet, G. Kelloff and K. Christov, Neoplastic transformation of mammary epithelial cells in rats is associated with decreased apoptotic cell death. *Carcinogenesis* **21**, 227-233 (2000).
59. ICRU, *Tissue Substitutes in Radiation Dosimetry and Measurement*. Report 44, International Commission on Radiation Units and Measurements, Bethesda, MD, 1989.
60. M. J. Berger, J. S. Coursey and M. A. Zucker (2000), *ESTAR, PSTAR, and ASTAR: Computer Programs for Calculating Stopping-Power and Range Tables for Electrons, Protons, and Helium Ions* (version 1.2.2). [Online] Available:

http://physics.nist.gov/Star [2005, May 30]. National Institute of Standards and Technology, Gaithersburg, MD.

61. ICRU, *Stopping Powers and Ranges for Protons and Alpha Particles*. Report 49, International Commission on Radiation Units and Measurements, Bethesda, MD, 1993.
62. S. Agostinelli, J. Allison, K. Amako, J. Apostolakis, H. Araujo, P. Arce *et al.*, Geant4: A simulation toolkit. *Nucl. Instrum. Methods Phys. Res.* **506**, 250-303 (2003).
63. K. F. Eckerman, M. Cristy, and J. C. Ryman, *The ORNL Mathematical Phantom Series*. Oak Ridge National Laboratory Report, available at http://homer.hsr.ornl.gov/VLab/VLabPhan.html, 1996.
64. ICRU, *Photon, Electron, Proton and Neutron Interaction Data for Body Tissues.* Report 46, International Commission on Radiation Units and Measurements, Bethesda, MD, 1992.
65. E. J. Bernhard, A. Maity, R. J. Muschel and W. G. McKenna, Effects of ionizing radiation on cell cycle progression. *Radiat. Environ. Biophys.* **34**, 79-83 (1995).
66. A. Hwang and R. J. Muschel, Radiation and the G2 phase of the cell cycle. *Radiat. Res.* **150** (Suppl.), S52- S59 (1998).
67. R. Rowley, E. N. Phillips and A. L. Schroeder, The effects of ionizing radiation on DNA synthesis in eukaryotic cells. *Int. J. Radiat. Biol.* **75**, 267-283 (1999).
68. H. N. Cho, S. J. Lee, S. H. Park, Y. J. Lee, C. K. Cho and Y. S. Lee, Overexpression of heat-shock protein 25 augments radiation-induced cell-cycle arrest in murine L929 cells. *Int. J. Radiat. Biol.* **77**, 225-233 (2001).

69. J. Savell, S. Rao, W. J. Pledger and W. Wharton, Permanent growth arrest in irradiated human fibroblasts. *Radiat. Res.* **155**, 554-563 (2001).

70. M. Verheij and H. Bartelink, Radiation-induced apoptosis. *Cell Tissue Res.* 301, 133-142 (2000).

71. N. Shinomiya, New concepts in radiation-induced apoptosis: 'Premitotic apoptosis' and 'postmitotic apoptosis'. *J. Cell. Mol. Med.* **5**, 240-253 (2001).

72. F. Ianzini, R. Cherubini and M. A. Mackey, Mitotic catastrophe induced by exposure of V79 Chinese hamster cells to low-energy protons. *Int. J. Radiat. Biol.* **75**, 717-723 (1999).

73. S. D. Griffiths, S. J. Marsden, E. G. Wright, M. F. Greaves and D. T. Goodhead, Lethality and mutagenesis of B lymphocyte progenitor cells following exposure to α-particles and X-rays. *Int. J. Radiat. Biol.* **66**, 197-205 (1994).

74. E. J. Hall, *Radiobiology for the Radiologist*, Lippincott Williams & Wilkins, Philadelphia, 2000.

75. N. Foray, C. F. Arlett and E. P. Malaise, Underestimation of the small residual damage when measuring DNA double-strand breaks (DSB): Is the repair of radiation-induced DSB complete? *Int. J. Radiat. Biol.* **75**, 1589-1595 (1999).

76. J. F. Ward, The yield of DNA double-strand breaks produced intracellularly by ionizing radiation: A review. *Int. J. Radiat. Biol.* **57**, 1141-1150 (1990).

77. J. P. Banath, M. Fushiki and P. L. Olive, Rejoining of DNA single- and double-strand breaks in human white blood cells exposed to ionizing radiation. *Int. J. Radiat. Biol.* **73**, 649-660 (1998).

78. L. Metzger and G. Iliakis, Kinetics of DNA double-strand break repair throughout the cell cycle as assayed by pulsed field gel electrophoresis in CHO cells. *Int. J. Radiat. Biol.* **59**, 1325-1339 (1991).

79. H. Mozdarani and P. E. Bryant, Induction and rejoining of chromatid breaks in X-irradiated A-T and normal human G2 fibroblasts. *Int. J. Radiat. Biol.* **56**, 645-650 (1989).

80. D. Blocher, DNA double-strand break repair determines the RBE of alpha-particles. *Int. J. Radiat. Biol.* **54**, 761-771 (1988).

81. P. L. Olive, DNA damage and repair in individual cells: Applications of the comet assay in radiobiology. *Int. J. Radiat. Biol.* **75**, 395-340 (1999).

82. N. Foray, C. Monroco, B. Marples, J. H. Hendry, B. Fertil, D. T. Goodhead, C. F. Arlett and E. P. Malaise, Repair of radiation-induced DNA double-strand breaks in human fibroblasts is consistent with a continuous spectrum of repair probability. *Int. J. Radiat. Biol.* **74**, 551-560 (1998).

83. J. Fulford, H. Nikjoo, D. T. Goodhead and P. O'Neill, Yields of SSB and DSB induced in DNA by Al(K) ultrasoft X-rays and alpha-particles: Comparison of experimental and simulated yields. *Int. J. Radiat. Biol.* **77**, 1053-1066 (2001).

84. A. H. W. Nias, *An Introduction to Radiobiology,* 2nd ed. Chichester, John Wiley & Sons, New York, 1998.

85. W. K. Sinclair and R. A. Morton, X-ray sensitivity during the cell generation cycle of cultured Chinese hamster cells. *Radiat. Res.* **29**, 450-474 (1966).

86. W. K. Sinclair, Cyclic x-ray responses in mammalian cells in vitro. *Radiat. Res.* 33, 620-643 (1968).

87. P. A. Thomas, B. L. Tracy, T. Ping, M. Wickstrom, N. Sidhu and L. Hiebert, Relative biological effectiveness (RBE) of 210Po alpha-particles versus X-rays on lethality in bovine endothelial cells. *Int. J. Radiat. Biol.* 79, 107-118 (2003).

88. I. Y. R. Adamson, Cellular kinetics of the lung. In *Toxicology of Inhaled Materials* (H. P. Witschi and J. P. Brain, Eds.) pp. 289-317. Springer-Verlag, Berlin, 1985.

89. P. Bolduc and L. Reid, Mitotic index of the bronchial and alveolar lining of the normal rat lung. *Am. Rev. Respir. Dis.* **114**, 1121-1128 (1976).

90. H. Spencer and R. G. Shorter, Cell turnover in pulmonary tissues. *Nature* **194**, 880 (1962).

91. N. H. Harley, Interaction of α particles with bronchial cells. *Health Phys*. **55**, 665-669 (1988).

92. A. Becciolini, M. Balzi, D. Fabbrica and C. S. Potten, Cell kinetics in rat small intestine after exposure to 3 Gy of gamma-rays at different times of the day. *Int. J. Radiat. Biol.* **70**, 281-288 (1996).

93. C. S. Potten, G. Owen and S. A. Roberts, The temporal and spatial changes in cell proliferation within the irradiated crypts of the murine small intestine. *Int. J. Radiat. Biol.* **57**, 185-199 (1990).

# VITA


| | |
|---|---|
| Name: | Natela Grigoryevna Ostrovskaya |
| Address: | 129 Zachry Engineering Building, MS 3133, Texas A&M University, College Station, TX 77843-3133 |
| Email Address: | natela@cedar.tamu.edu |
| Education: | B.S., Applied Mathematics, Obninsk Institute of Nuclear Power Engineering, Russia, 1997<br>Ph.D., Nuclear Engineering, Texas A&M University, 2005 |